CHALMERS
UNIVERSITY OF TECHNOLOGY

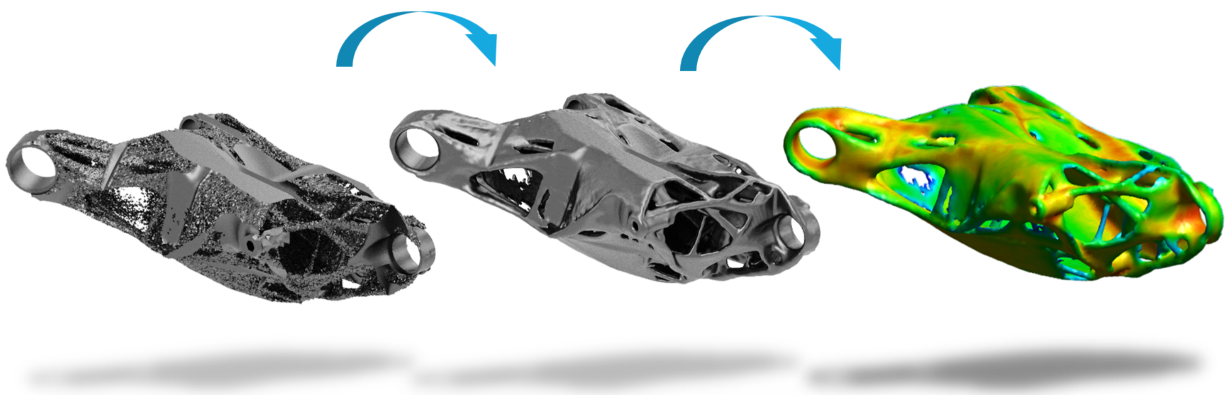

Development Process of Topology Optimized Casted Components

Master's Thesis in Applied Mechanics

NADINE KÅMARK

Department of Industrial and Materials Science
CHALMERS UNIVERSITY OF TECHNOLOGY
UNIVERSITY OF GOTHENBURG
Gothenburg, Sweden 2018

Master's thesis 2018

Development Process of Topology Optimized Casted Components

NADINE KÅMARK

Department of Industrial and Materials Science
Chalmers University of Technology
University of Gothenburg
Gothenburg, Sweden 2018

Development Process of Topology Optimized Casted Components
NADINE KÅMARK

Master's Thesis 2018
Department of Industrial and Materials Science
Division of Material and Computational Mechanics
Chalmers University of Technology and University of Gothenburg
SE-412 96 Gothenburg
Telephone +46 31 772 1000

Cover:
Illustrative picture of a topology optimized design getting transferred into a casting simulation result.

Gothenburg, Sweden 2018

Development Process of Topology Optimized Casted Components
Master Thesis in Applied Mechanics
NADINE KÅMARK
Department of Industrial and Materials Science
Chalmers University of Technology

Abstract

Both weight optimization and casting as a manufacturing method is widely used in the industry today. Topology optimization, as a weight optimization approach, is used to design lighter and more competitive components. Meanwhile, casting is a time and cost-efficient manufacturing method with the capacity to create complex shapes. Today, castability is not taken into account until the end of the development process. When the design is adjusted to become feasible to cast, mass is added which does not necessarily contribute to improve the structural strength. Thus, the structure is no longer optimized. Casting simulations assist in evaluating castability, but generally require animations and pictures to be analyzed manually.

At Volvo Cars and within the Re-OPTIC project founded via LIGHTer, there is an interest in finding methods to evaluate castability in the early phase of the development process. The purpose of this thesis is therefore to find a way of evaluating castability numerically, in order to be able to compare design concepts in the early phase of the development process. A process where optimization results can be casting-simulated, without manually realizing the design using CAD, is also presented in this thesis. Furthermore, the topology optimization manufacturing constraints *member size control* and *draw direction* are evaluated from a weight perspective, as well as a discretization improvement tool and the usage of two design spaces. This thesis is only considering the casting solidification process. The topology optimization work is carried out in the commercial software OptiStruct. The casting simulations is obtained using the commercial software Click2Cast.

Keywords: Weight Topology Optimization Casting Castability Solidification Simulation Development Process

Preface

This master thesis in Applied Mechanics at Chalmers University of Technology compromises 30 credits and was carried out at Altair and Volvo Cars in Gothenburg during the the autumn 2017. The examiner and academic supervisor was Martin Fagerström Associate Professor at the Division of Material and Computational Mechanics, Chalmers University of Technology. The supervisors in industry were Magnus Lundgren and Johan Dahlberg at Altair, Gothenburg. The supervisors in industry were also Harald Hasselblad and Andreas Carlsson at Volvo Cars, Gothenburg. This thesis has been a part of the Re-OPTIC program by LIGHTer.

Abbreviations

RLCA	Rear Lower Control Arm
FE	Finite Element
FEA	Finite Element Analysis
HW	HyperWorks
HM	HyperMesh
CAD	Computer Aided Design
C2C	Click2Cast
SIMP	Solid Isotropic Material with Penalization
MBS	Multi Body Simulations
TempGrad	Temperature Gradient
SW	Shrink Wrap
DS	Design Space

Contents

List of Figures

List of Tables

1| Introduction

1.1 Background

Both weight optimization and casting as a manufacturing method is widely used in the industry today. Weight optimization is used by design engineers in the development process to produce lighter and more competitive components. Meanwhile, casting is a time and cost-efficient manufacturing method which offers the opportunity to create complex shapes with relatively simple tools [1].

Today, design engineers are not fully taking into account the cast manufacturing requirements and restrictions in the development process [1]. The casting simulation tools are mainly used by the foundry engineers to predict the castability of a component. The foundry engineers usually have to add material to make the weight-optimized component feasible to cast. The added mass only benefits the casting process and does not improve the structural strength of the component [2].

A schematic flowchart of today's development process is illustrated in Figure 1.1. As shown, there is no iteration between the weight optimization and cast optimization processes.

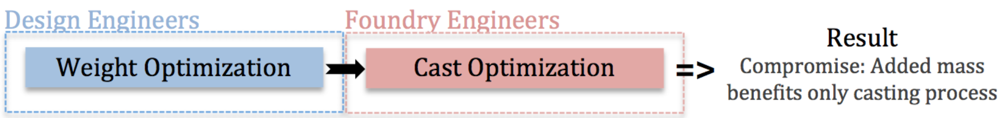

Figure 1.1: Schematic flowchart of the current development process of weight optimized casted components.

Topology optimization is one of the structural optimization approaches that can be used for weight optimization (see Section 2.1). In particular topology-optimized results become difficult to cast since the topology-optimized structure becomes very complex, especially if no manufacturing constraints are considered.

This master thesis is based on a previous master thesis "Methodology for Topology and Shape Optimization: Application to a Rear Lower Control Arm (RLCA)" by Robin Larsson [2]. The RLCA is one of the parts in the rear wheel suspension of a Volvo car. The RLCA is today manufactured using casting with a sand core and about five casting ingates and are made in aluminum [2]. More information about the current development process of the RLCA can be found in Robins thesis [2]. The Optimized Design became 22.5% lighter compared to the Current RLCA (see Figure 1.2).

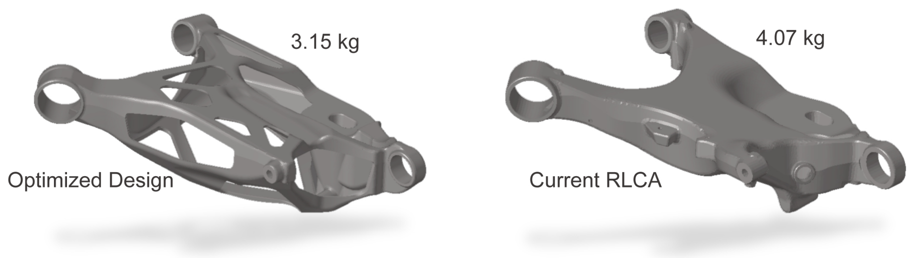

Figure 1.2: Picture of the Optimized Design (left) and the Current RLCA (right).

However, in order to make the Optimized Design feasible to cast, the foundry engineers needed to add additional material to the component which increased the total mass to 4 kg.

In an ordinary casting process this kind of problem are reduced by having a design engineer, a tools engineer and a foundry engineer working together to reach an acceptable result [20]. Though, since large industries most commonly does not pick their foundry until the development process already is accomplished, i.e. when the component already is designed, new strategies have to be developed.

Several previous studies have been done to understand which factors that are affecting the castability [3]. There also exist a lot of different methods of how to examine a casting to evaluate the performance and to understand what should be changed to improve the result [4][5]. While there are hardly any studies of how to evaluate castability in a numerical way using casting simulations.

Yet, there is no automated process to convert a topology result into a CAD-model. This problem is further described in [6][7]. Interested readers are also referred to the doctoral thesis "Finite element methods for surface problems" where Cenanovic aim to solve this problem with a different and very interesting approach [8], which differs from the element density theory that is used in OptiStruct.

1.2 Purpose and aim

The purpose of this master thesis is to find an efficient development process for topology optimized casted components, where casting simulations and manufacturing constraints will be integrated in the early phase of the ordinary optimization process.

As illustrated in Figure 1.3, the aim is to find an iterative process where the design engineers can use casting simulation as a tool to evaluate the castability, without having to realize the topology result. Since the realization process is very time consuming due to the manual modelling of creating a CAD model out of the topology result, lead times can be reduced by avoiding the realization part in the iterative process. It is also of interest to find a way to sort among a large variety of different design concepts by evaluating castability in a numerical way.

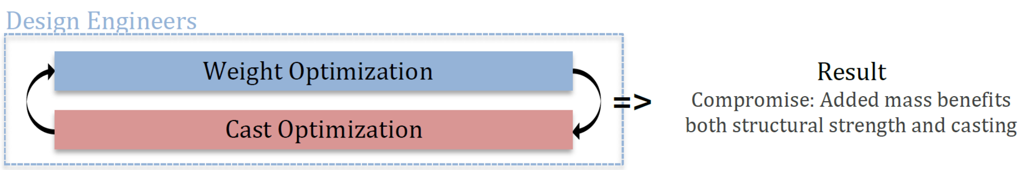

Figure 1.3: Preferred development process of weight optimized casted components.

The work has been carried out with Altair and Volvo Cars as a part of the Re-OPTIC project by LIGHTER. An existing product, a rear lower control arm, is used throughout the project. The results are expected to be generic and applicable on other components and in other industries.

Software provided by Altiar has been used during this master thesis project. HyperMesh 2017.2 has been used for pre-processing the finite element (FE) models. The finite element analysis (FEA) and optimization problem has been solved by OptiStruct 2017.2.

The casting simulations have been solved and post-processed using Click2Cast 4.1 (C2C). HyperView 2017.2 has been used for post-processing both optimization results, FE-results and casting simulation results.

1.3 Limitations

Casting simulations are divided into two parts, form filling simulation and solidification simulation. Only solidification simulations will be considered during this project due to the large amount of input data that are required to run a form filling simulation and due to the fact that the form filling simulation require the casting method to be pre-specified. Furthermore, in order to narrow down the work, neither gas porosity, different mold materials nor the shakeout time is considered in this thesis work.

Not all of the topology optimization results is investigated from a casting point of view, due to the time frame of this thesis. Only the unconstrained topology optimization and one of the topology optimization results using manufacturing constraints are investigated with respect to castability.

No particular cost aspects is considered apart from minimizing the usage of casting tools (such as in-gates, chillers, feeders etc [9]) and lead times which indirectly will cut down the developing and production costs.

Only linear static structural analysis is performed in this thesis. Neither eigenfrequencies nor fatigue is considered.

2| Theory

The relevant theory of the thesis is presented in this chapter. Firstly, a brief explanation of structural optimization is presented followed by the theory behind topology optimization. Secondly the theory behind casting, casting simulation and its application in HyperWorks is presented.

2.1 Introduction to Structural Optimization

A structural optimization problem is composed of an objective function (f), design variables ($\mathbf{x}$) and state variables ($\mathbf{y}$). The objective function represents the objective to be either minimized or maximized during the optimization. For example, the objective function f could be measuring weight, effective stress or displacement in a given direction. The design variables can be both functions or vectors that describe the design, usually the geometry which are varied during the optimization until the optimal set of the design variables is found and yields the optimal value of the objective function.[10]

A general expression of the structural optimization problem can be stated as follows:

$$(opt)\begin{cases}\text{min f}(\mathbf{x},\mathbf{y}) \text{ with respect to } \mathbf{x} \text{ and } \mathbf{y} \\ \text{subject to} \begin{cases}\text{constraints on } \mathbf{y} \\ \text{constraints on } \mathbf{x} \\ \text{equilibrium constraint}\end{cases}\end{cases} \tag{2.1}$$

There are three types of structural optimization problems: sizing optimization, shape optimization and topology optimization. This report will focus on topology optimization. For further reading about size and shape optimization see [10].

2.1.1 Topology Optimization

The theory in this chapter describes topology optimization in general terms and how it is applied in OptiStruct. Topology optimization is about finding the optimal placement of the material within a specified region to reduce weight without violating the structural requirements.

2.1.1.1 Problem formulation and FE-discretization

The pre-defined region (Ω) to be optimized is usually called the design domain, design volume or design space, meanwhile Ω_{mat} is the sought optimal subset of the design volume Ω. To solve the topology optimization problem numerically, a discretization of the problem using the finite element (FE) method is required. The optimization, Eqs. (2.2-2.4), aims to find the minimum mass, subjected to the equilibrium constraint, Eq. (2.4), and an upper boundary constraint C_{bc} on the compliance, Eq. (2.3). The expressions are stated in the general discrete problem formulation [11]:

$$\min_{\rho_e} \int_{\Omega} \rho_e \, d\Omega = vol(\Omega_{mat}) \leq \Omega \tag{2.2}$$

in order that

$$C(\boldsymbol{\rho}) = \mathbf{f}^T \mathbf{u} \leq C_{bc} \tag{2.3}$$

s.t

$$\mathbf{K}(\rho_e)\mathbf{u} = \mathbf{f} \tag{2.4}$$

where $\mathbf{u}$ contains the displacement degrees-of-freedom for each node, $\mathbf{f}$ is the load vector and $\mathbf{f}^T\mathbf{u}$ is the compliance C which is the inverse of the stiffness. $\mathbf{K}$ in the equilibrium equation (2.4) is the global stiffness matrix. The stiffness matrix $\mathbf{K}$ depends on the densities ρ_e in each element e where $e = 1, ..., N$ and N is the total number of elements of the meshed design space. The stiffness matrix $\mathbf{K}$ is defined as:

$$\mathbf{K} = \sum_{e=1}^{N} \mathbf{K}_e(\rho_e) \tag{2.5}$$

Where the element densities ρ_e can vary between 0 and 1. For $\rho_e = 1$ the element is filled whereas $\rho_e = 0$ represents a void element [2].

To solve the topology optimization problem a penalization method known as the SIMP (*Solid Isotropic Material with Penalization*) method is used. SIMP is a structural optimization density method based on the finite element method. It is used to solve the binary density problem by modelling the densities, through interpolation, with continuous functions so that the densities can vary between 1 and 0 [2][6][10][21]. This is done by applying a so called pseudo density parameter (penalization parameter) to each element of the FE-mesh. The density function can be expresses as:

$$\bar{\mathbf{K}}(\rho_e) = \rho_e^p \mathbf{K}, \ \ \rho_e \in [\rho_{e,min}, 1], \ \ p > 1 \tag{2.6}$$

where $\bar{\mathbf{K}}$ represents the penalized stiffness matrix, $\mathbf{K}$ the real stiffness matrix, ρ_e the element density and p the penalization factor which is always greater than 1 [2][6][10][21] and usually takes a value between 2.0 and 4.0 [15]. For further reading about the SIMP-methodology, see [6].

2.2 Casting

Casting is a manufacturing process where liquefied metal is poured into a mold and thereafter solidified into a solid metal piece with the same shape as the hollow cavity of the mold. The solidified piece, also known as the casting, is then recovered from the mold. There are a lot of different casting methods such as gravity casting, die casting, high and low-pressure casting, investment casting etc. For further information about casting methods see [1][22].

The casting system can be rigged in several different ways. Mainly depending on the particular component design and its features, but also depending on the foundry since each foundry usually have their own preferences. Some of the most essential components of a casting system are the mold (cope and drag), sprue, runner, risers (also known as feeders) and core, illustrated in Figure 2.1. A core can be used to create an interior shape of the model and are commonly used in sand casting [9]. Very complex sand casting molds and cores can today be produced using 3D printing. Furthermore, both molds and the castings can be made of different materials.

Large castings usually require a gating system (Figure 2.2) with multiple in-gates to be properly fed. The main purpose of a gating system is to ensure that enough liquid metal reaches the mold cavity, but gating systems are also used to control shrinkage and can also be designed to minimize turbulence during the filling [22]. For more details about the casting system see [9][22].

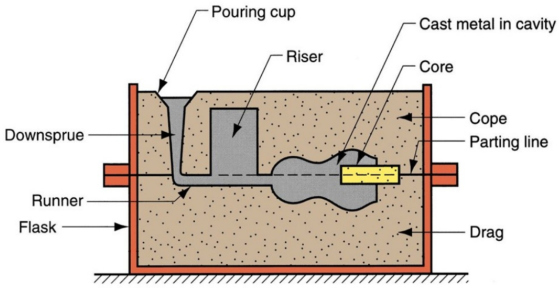

Figure 2.1: Rigging system for casting.

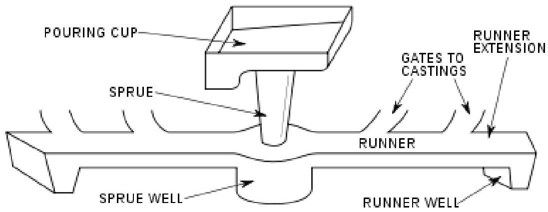

Figure 2.2: Gating system [22]

The variation of the microstructure yields worse mechanical properties of a casting compared to products manufactured using extrusion, rolling or forging, where the machining work refines the microstructure which improves the mechanical properties [3]. There are many parameters that affect the mechanical properties of a casting. Apart from reduced casting defects, a fast solidification for example leads to improved mechanical properties due to the fact that a finer dendrite structure are produced during the solidification, which are further described in [3][12][17][18]. Though, it is not the total solidification time that matters physically, but the local solidification rate. A restricted amount of casting defects, i.e. worsen mechanical properties, can permitted as long as the defects does not occur within stress intense zones in the structure. Today design engineers mark critical stress zones and send it to the foundries in order to inform the foundry engineers where casting defect has to be restricted.

2.2.1 Cast shrinkage defects

Casting defects are mainly controlled by fluid flow, heat transfer and thermal stresses. Gas porosity, shrinkage defects, mold material defects, pouring metal defects and metallurgical defects are five of the casting defect categories [22]. The shrinkage defects can be divided into: solidification shrinkage, liquid shrinkage and patternmaker's shrinkage [22]. This project will mainly focus on the solidification shrinkage defects.

Solidification shrinkage occurs due to the fact that metals are less dense in the liquid phase compared to their solid state [22]. As a consequence, liquid metal will shrink during the solidification. Unless more liquid is provided, so called shrinkage porosity will arise. Shrinkage defects are usually divided into the two different categories: closed shrinkage defects and open shrinkage defects [13]. Open shrinkage defects appear on the surface of the casting meanwhile the closed shrinkage defects also known as shrinkage porosity are formed within the casting. Shrinkage porosity can be predicted in so-called hot spots. Hot spots are regions where liquefied metal becomes isolated within already solid material.

2.2.2 Castability

Castability describes the ability of producing a casting without any defects. Today there is no definite and accurate way to quantify castability. Furthermore, there is only a limited number of ways to evaluate a geometry numerically from a casting point of view. The Equations (2.7) - (2.9) can be used as indicators of whether a geometry is feasible to cast. The design of a component, or more specific, the volume, the surface area and the number of features are used to evaluate castability, where a large value on c_1, c_2 and c_3 implies good castability.

$$c_1 = \frac{V_c}{V_b} \tag{2.7}$$

Here V_c is the volume of the casting, V_b is the volume of the smallest box that the casting can fit in and A_c is the surface area of the casting.

$$c_2 = \frac{6(V_c)^{2/3}}{A_c} \tag{2.8}$$

n_f is the number of features of the casting, i.e. number of holes, ribs, slots, pockets etc.

$$c_3 = \frac{1}{(1 + n_f)^{0.5}} \tag{2.9}$$

Even though there is no straightforward and general approach of how to quantify castability, there is a lot of recommendations and rules of how a component should be designed to make it feasible to cast. For example, a casting should be designed in such way so that it induces a suitable directional solidification with respect to the in-gates. This is called directional solidification and implicates that the solidification works its way towards the in-gate from the farthest end of the casting [23]. A taped design will benefit the directional solidification due to the fact that the solidification moves from thin to thicker regions [20][1]. This can be proved and explained by the Chvorinov's rule (Eq. 2.10). Chvorinov's rule declare the relation between the solidification time t_s and the solidification modulus M (Eq. 2.11), where the solidification modulus is a function of the geometry as the volume-to-surface-area ratio [12]. Chvorinov's rule is based on the 1D heat transport across the material and mold interface [12].

$$\text{Chvorinov's rule: } t_s = C\left(\frac{V}{SA}\right)^2 \tag{2.10}$$

Where C is a constant and depends on the mold and material properties [24].

$$\text{Solidification Modulus: } M = \frac{V}{SA} \tag{2.11}$$

Furthermore, a casting should be designed in such way that it can be properly fed. For example, the minimum member size of an aluminum alloy casting is 5 mm according to [18]. Abrupt changes of the wall thickness affect the castability negatively since it leads to turbulence during filling. This can be avoided by adding a radius on all corners and edges, i.e. to use so-called fillets [22]. Thin sections should not be placed in-between thick sections and adjacent to entrances of risers [1]. It is also of importance to avoid isolated thick sections that are difficult to feed [1]. There are several casting design rules presented in [1], where for example relations between the thicknesses in a junction are stated (Figure 2.3).

It has been observed that porosity can be minimized by keeping the temperature gradient as low as possible over the structure [3][12]. Unfortunately there is yet no critical threshold value for the temperature gradient[3], besides a proposed "geometric" model for a plate by Sigworth and Wang (1993) [12].

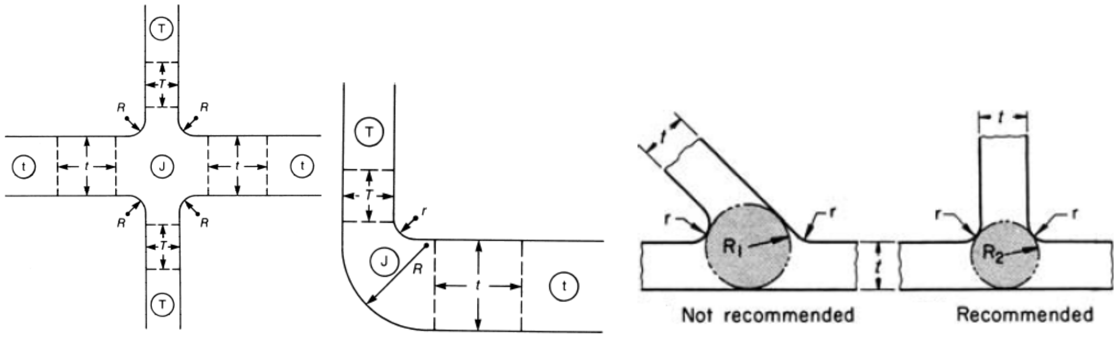

a) X-section. b) L-junction. c) T- versus Y-junction.

Figure 2.3: Models of different junctions [1]. Casting design rules.

2.2.3 Solidification simulation

Casting simulations allow engineers to make virtual castings instead of using trial and error methods, by actually making the casting, to find the optimal processing parameters [3]. Casting simulations are divided into form filling simulation and solidification simulation. When both filling simulation and solidification simulation are calculated in C2C, the temperature distribution from the end of the filling simulation is used as the starting temperature of the solidification analysis [9]. Whereas only the solidification is calculated, the simulation assumes that the mold is perfectly filled and will use a homogeneous starting temperature at the beginning of the solidification process [1][9]. It should be taken into account that this simplification can be a crucial source of errors [12]. In C2C it is required to pick an inlet regardless of the simulation type. Only the differences of the heat coefficient at the inlet area will affect the solidification result, i.e. a small inlet will affect the result less than a large inlet. The solidification simulation in C2C does not consider the gravity effect. The solidification simulation generates results such as temperature, liquid fraction, solidification time, Niyama values, solidification modulus, porosity percentage, porosity, etc.

Liquid fraction gives the possibility to predict where shrinkage porosity will occur by analyzing the animation and track areas where liquid spots becomes isolated within already solid material, so called hot spots. Liquid fraction is based on the temperature gradients which are determined by the direction of the temperature change and are therefore commonly used by foundry engineers to control directional solidification.

Niyama is a porosity criterion used by foundry engineers to detect solidification shrinkage defects [9]. The Niyama function expresses the pressure drop in the mushy region as a function of $G/R^{1/2}$ at the end of the solidification [3], where the local cooling rate R and the local temperature gradient G are determined according to equation (2.12) and (2.13) respectively.

$$\text{Cooling Rate, } R = \frac{\Delta T}{\Delta t_s} \tag{2.12}$$

$$\text{Temperature Gradient, } G = \sqrt{G_{0x}^2 + G_{0y}^2 + G_{0z}^2} \tag{2.13}$$

$$G_{0x} = \frac{1}{n}\sum_{1}^{n}\frac{\Delta T_i}{\Delta x_i}, \text{ where } \; i = 1, 2, 3... \tag{2.14}$$

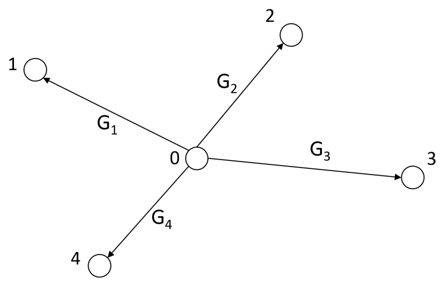

Figure 2.4: Schematic figure of how the temperature gradient is calculated based on the neighboring nodes.

Figure 2.5 shows when during the end of the solidification time the temperature gradient G and the cooling rate R can be calculated. The critical Niyama range are different for different materials. For Aluminum it stretches from 0 to 0.3, where a lower value indicates higher probability of shrinkage [9].

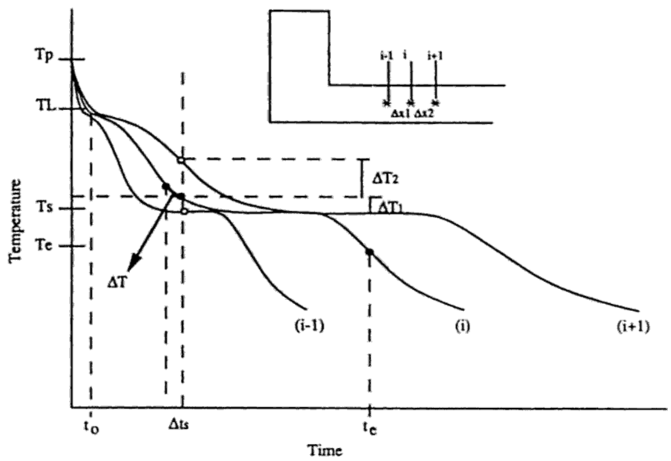

Figure 2.5: Thermal parameters during the solidification used for the Niyama criteria function [3].

As mentioned in Subsection 2.2.2 the solidification modulus, also known as the geometrical modulus, is a function of the geometry as the volume-to-surface-area ratio (Eq. 2.11). The total solidification modulus is easily calculated using the total volume divided by the total surface area. The solidification modulus within the structure on the other hand would be far more difficult to determine without the Chvorinov's equation (2.10). C2C uses Chvorinov's equation by extracting the solidification modulus M and make it a function of the final solidification time in each node (Eq. 2.15).

$$M(t_s) = \sqrt{\frac{t_s}{C}} \tag{2.15}$$

3| Method

Pre-literature studies were carried out in order to achieve a general understanding and knowledge within the subject. Hence, the project was divided into four sub parts:

- Topology optimization (3.1)
- Topology result into casting simulation (3.2)
- Evaluating castability (3.3)
- Re-optimization

The re-optimization refers to the situation when the most optimal design concept has been found but still has to be slightly modified. Further investigations has to be done to determine how these modifications should be performed in order to still maintain an optimal design from both a strength and a castability point of view.

This master thesis has been focusing on the first three parts, which are presented and further described in each of the following Sections 3.1-3.3. The method of how the results from Section 3.1-3.3 was concluded is described in Section 3.4. An overall working procedure of the development process for topology optimized casted components was finalizing this project and is presented in Chapter 7.

3.1 Topology Optimization

3.1.1 Topology optimization in OptiStruct

When the topology optimization problem in OptiStruct was defined, the first step was to specify the design space (DS), the so-called none design space and the loads. The predefined design space that has been used in this project is shown in Figure 3.1. The darker parts in Figure 3.1 are the non design spaces where the loads were connected.

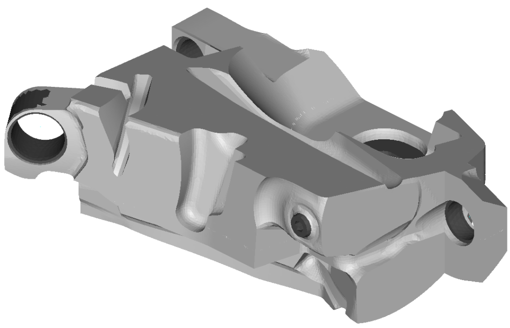

Figure 3.1: Design space, which is a solid volume. The dark regions are were the loads and constraints are connected.

The load cases were provided by Volvo Cars and have been generated by Multi Body Simulations (MBS) of a full vehicle. The load cases describe different events such as drive over curb (DOC), skid against curb (SAC), brake in pothole (BIP) and rearwards driving over curb (ROC). In total 21 different load cases were used. For more information about the load cases, see [2].

The objective function was set to minimizing the total mass and an upper bounds was applied on the compliance for each load case. These compliance bounds were implemented as displacement constraints derived from the stress analysis of the Current RLCA. Thus, for each load case, the displacements of the load introduction points were obtained in the stress analysis of the Current RLCA and then used as upper bounds in the optimization. Thus, the mass will be minimized meanwhile the structural stiffness will be conserved in relation to the Current RLCA. All topology optimization in this thesis will have the same objective function and constraints.

Within OptiStruct one have the ability to define different manufacturing constraints, such as stamping, extrusion, symmetry, draw direction etc. Although, one initially use to run an optimization without any manufacturing constraints, a so called unconstrained topology optimization.

In addition to running an unconstrained topology optimization, which would result in the lightest and most optimal design from a strength perspective, it was also of interest to investigate which optimization controls and manufacturing constraints that could be used to get a feasible design from a casting point of view. The manufacturing constraints member size control MINDIM and draw directions, with or without holes, as well as the optimization control TOPDISC were investigated. Furthermore, the usage of two design spaces, to illustrate a core and to get a cavity in the middle of the casting, was studied (see Figure 3.2 for a total summary).

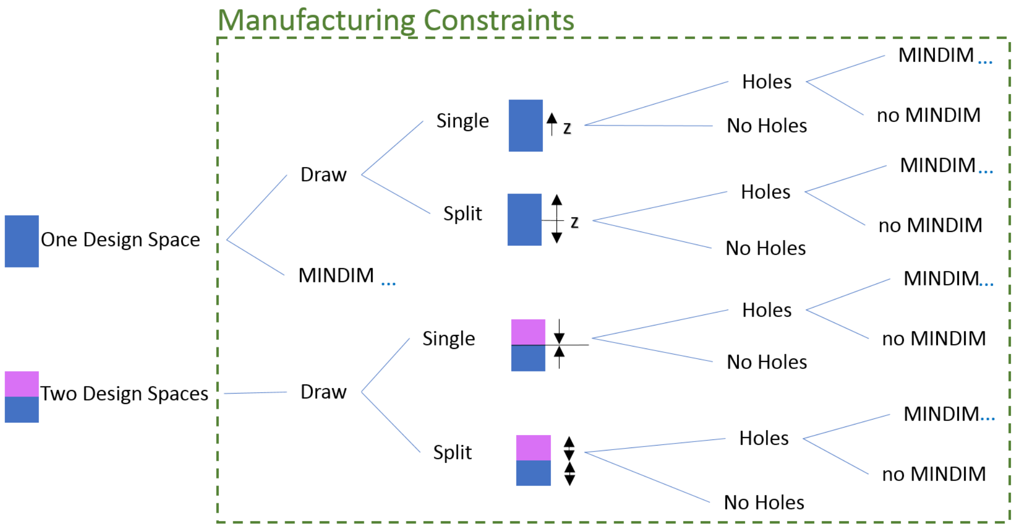

Figure 3.2: Manufacturing constraints that will be investigated during this project.

As explained in the limitation (Section 1.3), all of the topology optimization results were not evaluated from a casting point of view in this project due to the time frame of this master thesis. Only the unconstrained topology optimization together with one of the candidates using manufacturing constraints were further investigated.

3.1.2 Mesh dependence

Figure 3.3 shows that a finer mesh, i.e. a mesh with a lot of small elements, results in thinner walls compared to a coarse mesh with fewer and larger elements. A finer mesh will capture more details and will also result in a lower total mass. On the other hand, much faster calculations can be done when using a coarse mesh and is therefore recommended to be used for experimental optimization runs. A finer mesh is recommended to be used for final results.

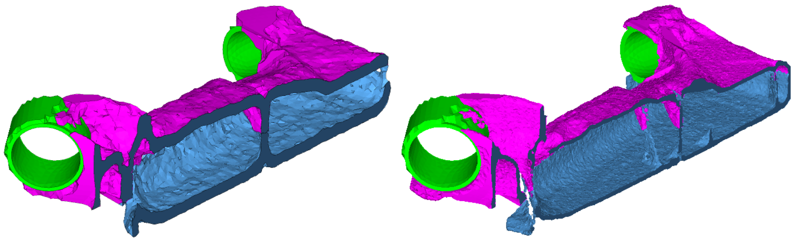

Figure 3.3: Mesh dependence.
Coarse mesh $x = 6$ mm (left) compared to a fine mesh $x = 3$ mm (right).

Element size [mm]	6	3
Weight [kg]	8.34	5.13
Nr of elements	600 851	8 320 344
Computation time [hh:mm:ss]	00:37:00	24:45:00
RAM [MB]	129 092	775 491
Nr of CPUs	24	24
Iterations	32	39

Table 3.1: Differences between a coarse mesh and a fine mesh.

Table 3.1 presents the differences in computation time of the models shown in Figure 3.3. As can be seen, the finer mesh gives far more elements which results in much longer computation time.

3.1.3 Draw direction applied in OptiStruct

A draw direction control can be used in OptiStruct in order to constrain the topology optimization with the purpose to allow the die to slide in a given direction. Either a *single* draw option or a *split* draw option can be used, see Figure 3.4. *single* draw represents one die sliding in a given direction meanwhile the *split* draw option implies that two dies are splitting apart in the given direction. The splitting line, i.e. the so called parting line, is optimized during the optimization [15].

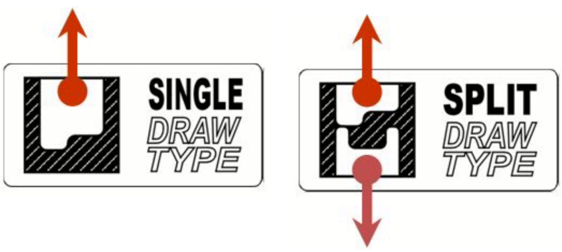

Figure 3.4: Optimization results when using different draw direction options: *single* and *split*.

3.1.4 MINDIM - Member size control applied in OptiStruct

MINDIM is an optimization control which provides an opportunity to specify the minimum diameter of the members formed in the topology optimization. It is mainly used to eliminate small members in the topology result, but can also be used to eliminate checkerboard results. MINDIM is required to take a value at least three times greater than the average element size ($\bar{x}$) and no greater than twelve times the average element size ($\bar{x}$).[15]

$$3 * \bar{x} < MINDIM < 12 * \bar{x} \tag{3.1}$$

where x is the element size and the average element size $\bar{x}$ for 3D elements is calculated as the average of the cubic root of the volume of the elements.

$$\bar{x} = \sum_{N=1}^{N} \sqrt[3]{V_i}/N = \frac{\sqrt[3]{V_{tot}}}{N} \tag{3.2}$$

N is the total amount of elements and V_i is the volume for element i where $i = 1, .., N$.

If the structure contains members which are slightly smaller than the specified MINDIM, but are very important for the load transmission, then these member-diameters will not be reduced. If a user-defined MINDIM value is greater than 12 times the average element size then MINDIM will be reset to be equal to 12 times the average element size. When draw direction constraints are activated, user-defined MINDIM values that are smaller than 3 times the average element size will be replaced by a MINDIM value of 3 times the average element size. Furthermore, even though no member size control are set, a MINDIM value of 2 times the average element size will be enforced if TOPDISC are activated.

3.1.5 TOPDISC - Discretization control applied in OptiStruct

When activating the TOPDISC optimization control an improved discrete formulation are applied with the purpose to produce more discrete results for all topology optimization runs including manufacturing constraints. This means that less semi-dense elements will be produced when using TOPDISC.[16]

3.1.6 Post processing in HyperWorks

The topology optimization generates a lot of different result files. The ones used in this project are described in this section, as well as the post processing tools OSSmooth, iso averaging method and Shrink Wrap.

The FEA and optimization problem formulations are stated in a text file (.fem) which are used as an input file to the OptiStruct solver. The .out, .sh, .h3d and .tcl file are some of the output files generated by OptiStruct. The .sh file is a shape file containing the densities of all elements from the last iteration. The OptiStruct out-file contains all information about the optimization set-up and the optimization run, including information such as number of iterations, computation time, error messages etc. The h3d-file is a binary OptiStruct result file. The tcl-file contains all elements organized in 10 sets with respect to the element density (i.e. in steps of 0.1). A .stl file (Standard Triangle Language) describes a triangulated surface where the triangles are defined by the unit normal and the vertices [25].

The OSSmooth tool in HyperMesh as well as the iso-surface export in HyperView gives the opportunity to generate an iso-surface which furthermore can be exported as a .stl file. The iso-surface can be treated with an averaging-method before the export from HyperView. As the name indicates, the averaging method calculates a nodal averaging of the element-based results. The averaging method can be applied on both contours plots and iso plots. Figure 3.5 presents the difference between a contour plot and an iso plot, with and without averaging method.
The OSSmooth is generally used for re-analysis. OSSmooth makes it possible to import the optimization result into the initial model, as a relatively smooth volume mesh, meanwhile

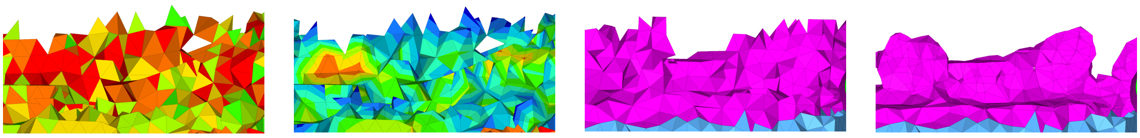

a) Contour: Non averaging. b) Contour: Averaging. c) Iso: Non averaging. d) Iso: Averaging.

Figure 3.5: Averaging method examples.

it keeps the connectivity to all loads. Before running the OSSmooth import, the user can specify a desired density threshold value (default=0.3).

Shrink Wrap (SW) is a tool in HyperMesh which generates an enclosed solid or volume based on a selected geometry. Shrink Wrap is usually used to simplify an existing model. Either a *tight* or *loose* Shrink Wrap can be used. The *loose* Shrink Wrap simplifies the geometry to a greater degree than the *tight* Shrink Wrap. The user has to specify the desired element size of the generated surface or solid mesh. Different setting combinations as well as using Shrink Wrap more than once were investigated.

3.2 Topology result into casting simulation

As mentioned in Section 1.2, the aim is to find a suitable method to get the topology result into the casting simulation without realizing the geometry by using CAD. As a matter of fact, the casting simulation does not actually require a CAD-model but needs a surface mesh as input. This makes it at least possible to postpone the CAD modelling to the end of the development process, i.e. when the final design has been selected, so that the realization only has to be done once. Nevertheless, the problem that still remains is that the topology optimization result is represented by volume elements with a rough surface meanwhile the casting simulation software needs a smooth surface mesh as input.

The HyperMesh tools Shrink Wrap and OSSmooth will be investigated, as well as the ISO-surface averaging method in HyperView.

3.3 Evaluating castability

It is necessary to find a way of analyzing and drawing conclusions from the cast results. Preferably in a numerical way since evaluations from neither pictures nor animations are as efficient or sufficiently consistent as when using numerical values.

To begin with, the Optimized Design and the Current RLCA were compared. This was done to get a better understanding of which conclusions that can be drawn from the simulation results, since it is already known that the Optimized Design was not feasible to cast. Hence, this was expected to be confirmed by using C2C. The same parameters were used in both cases so that the results could be compared equally. A detailed specification of the casting parameters are presented in Appendix A.

Extreme values are not necessary something bad when evaluating castability. Instead it is more about where different values occur and how it changes over the structure that can tell if the geometry is feasible to cast or not. Also the amount of critical areas are of bigger importance compared to the magnitude of the most critical value. For example, when looking at stresses, the maximum stress should not exceed the allowable stress limit, e.g. the yield limit. The focus will then be to decrease the maximum stress meanwhile the semi-critical stress regions are more or less ignored. Though, when it comes to casting results such as shrinkage porosity, a geometry with one spot with extremely high shrinkage porosity could be much more preferred than a lot of spots with semi high porosity. This is due to the fact that the shrinkage porosity in a spot can be reduced by placing an in-gate at this location, or by manipulating the solidification using relevant casting tools. Hence, one very critical spot is much easier and cheaper to deal with compared to a lot of semi-critical spots.

Liquid fraction shows the evolution of solidification presented as an animation (see Figure 3.6). In C2C the liquid changes from blue to red and then disappears when the material turns from liquid to solid.

Figure 3.6: Pictures captured from the animation sequence of the liquid fraction.

Due to the fact that it is neither efficient or consistent to make evaluations from animations, the temperature gradients presented in HyperView were investigated to see if it could be used to make evaluations based on numerical values instead. A tool called Envelope in HyperView was used to collect all the maximum values, in each node, over all time steps, and save it as a new substituted simulation result. The Envelope tool was also used for the stresses to collect the maximum stresses in each node for all 23 load cases.

A so called HotSpots tool in HyperView made it possible to search for regions with values over a specified threshold. The searching distance was specified as a diameter and the traced hot spots were presented in a table and in a plot.

Comparisons were only performed with results from FE-models created with the same element size, due to the fact that the volume porosity are based on the volume of each element. The fraction between the number-of-node result and the total number of nodes were always used for comparison, since the total amount of nodes differed between the models.

3.3.1 Stress mapping

How critical a certain amount of porosity is depends on where it occurs in relation to stress concentrations. Therefore, correlations between different casting results and stresses were investigated. It was believed that critical areas could be located very easily by deriving a new value for each node based on the cast results and the stress results in respective node. This could have been the case, if the stress results and the cast results were calculated based on the same mesh i.e. had exactly the same node numbering. But since only the surface mesh from the topology result were imported into C2C, and are thereafter volume-meshed with respect to the in-gate, a new mesh with different node numbering was generated to be used for the casting simulation. This problem was solved by converting the C2C mesh file into a OptiStruct bulk data format. By importing and connecting the loads to the new mesh, the stress analysis could then be performed on the new mesh with the same node numbering as the casting results. The converting was done by creating a converting script using the commercial software Compose (similar to MATLAB with the capability to directly read h3d result files).

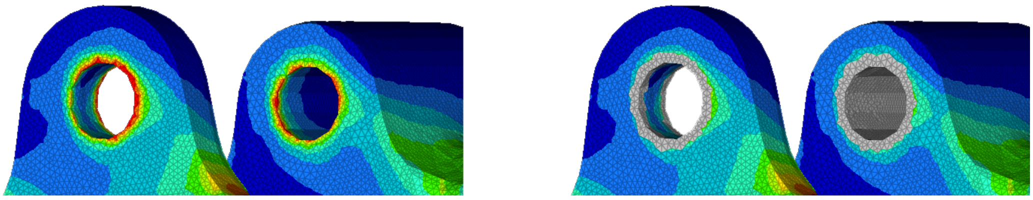

Figure 3.7: Left: unrealistic stress concentrations due to simplified bolt connections. Right: two layers of excluded element-results.

It is of importance to consider how the simplified bolt modeling technique using beam elements and rigid body elements (RBE) affects the stress results. The 1D elements, which were used to illustrate a bolt connection, resulted in a too stiff representation of a bolt which furthermore led to unrealistic stress concentrations in the adjacent elements, as shown in Figure 3.7. Therefore, two layers of the adjacent elements of each bolt connections were excluded in the stress results.

3.4 Conclusion and verification

At the end of this project a proposed work procedure should be stated. The results in Chapter 4 - 6 are summarized into a proposed development process for topology optimized casted components, presented in Chapter 7.

The weighted average of the evaluation results, such as critical porosity, Niyama values and stresses (denoted $K_{i,j}$ below), can be calculation by adding their values normalized with respect to maximum value of all design concepts considered (denoted j) for each criterion K_i (Eq. 3.3).

$$w_{i,j} = K_{i,j}/K_{i,max} \tag{3.3}$$

$$W_j = \sum_i w_{i,j} \tag{3.4}$$

i \ j	DC 1	DC 2	...	max	DC 1	DC 2	...
K1	$K_{1,1}$	$K_{1,2}$	$\dots$	$K_{1,max}$	$w_{1,1}$	$w_{1,2}$	$\dots$
K2	$K_{2,1}$	$K_{2,2}$	$\dots$	$K_{2,max}$	$w_{2,1}$	$w_{2,2}$	$\dots$
$\vdots$	$\vdots$	$\vdots$	$\ddots$	$\vdots$	$\vdots$	$\vdots$	$\ddots$
					W_1	W_2	

Table 3.2: Example of how the evaluation criteria was weighted.

These normalized values $w_{i,j}$ can then be summed up and examined in several different ways. Only two simple approaches was used in this thesis work. The first approach was to calculate the sum of all normalized values $w_{i,j}$ (including the mass) to get the rating value R_j (Eq. 3.5) for each design concept j. The lowest rating R_j indicates the best design concept. The other approach was to consider the mass equally important as the other criteria factors together $W_{j,excl\ mass}$ (Eq. 3.6 and 3.7).

$$R_j = \frac{W_j}{W_{max}} \tag{3.5}$$

$$W_j^* = \frac{W_{j,excl\ mass}}{W_{max}} + w_{mass,j} \tag{3.6}$$

$$R_j^* = \frac{W_j^*}{W_{max}^*} \tag{3.7}$$

4| Results Topology Optimization

A parameter study is conducted to see how the optimization results are influenced when the parameters TOPDISC and MINDIM are altering and when the draw direction manufacturing constraint are used. All results in this report has a density threshold of 0.3, which means that all the displayed elements have a density between 0.3 and 1 and all elements with a density less than 0.3 have been removed in the post-process. The weight has always been measured after the density of each element in the interval 0.3 - 1 has been set to 1. All results in this chapter will mainly be compared from a weight perspective.

4.1 Unconstrained topology optimization

The unconstrained topology optimization is presented in Figure 4.1. The design tends to form a shell structure with a couple of ribs in the middle, although it is hard to see from the pictures. Table 4.1 presents the weights of an unconstrained topology optimization using an element size of 3 mm and 6 mm. TOPDISC will always be deactivated for the unconstrained topology optimization since TOPDISC is only intended to be used for optimizations including manufacturing constraints.

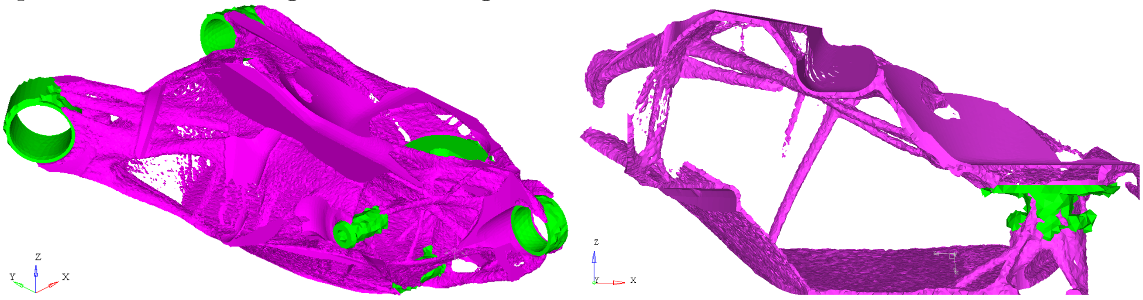

Middle section cut.

Figure 4.1: Pictures of the unconstrained topology optimization ($x = 3mm$).

Unconstrained		
Element size [mm]	3	6
Weight [kg]:	3.38	4.08
TOPDISC:	Off	Off

Table 4.1: Weight difference of the unconstrained topology optimization with different element sizes.

4.2 Draw direction

The results from the topology optimization with the initial set-up (see Section 3.1) in combination with the manufacturing constraints *split* draw and *single* draw direction are presented in this section. As well as the draw direction option *no holes*.

4.2.1 Split and Single draw direction

As shown in the Table 4.2 the *single* draw direction becomes significantly heavier than the *split* draw direction. This could be an outcome of the initial load cases i.e. depending on how the load paths are orientated. By looking at the unconstrained topology optimization (Figure 4.1) it can be seen that the load paths are following the outer boundary of the structure. Load paths spread out in the draw direction will result in lots of added material to fill the holes along the draw direction.

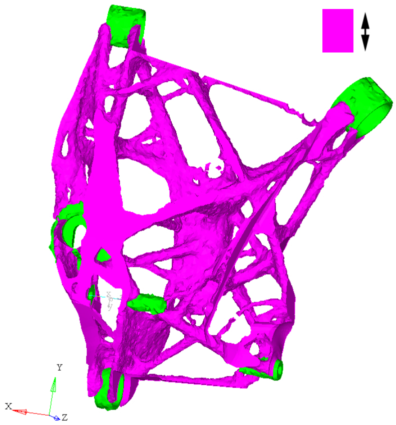

Figure 4.2: *split* draw direction.

Figure 4.3: *single* draw direction.

	Split	Single
Weight [kg]:	5.22	7.23
Element size [mm]:	6	6
No holes:	Off	Off

Table 4.2: Weight difference between *single* and *split* draw direction.

4.2.2 No holes: on or off

The outcome of using the *no holes* option is presented in this section. The *no holes* option is only provided when using manufacturing constraints.

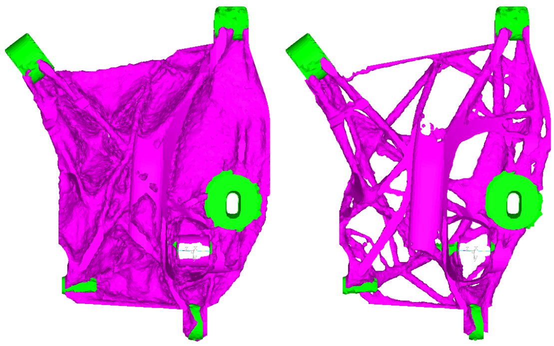

Figure 4.4: The *no holes* option is activated on the left and deactivated at the right hand side in this picture. Both models have an element size 6 mm and *split* draw direction on one design spaces.

Several optimization runs are performed and shows unambiguously that the activation of the *no holes* option only plugs all the holes in the structure with added mass, without changing the design any further. Thus, it make sense that the weight increases when activating the *no holes* options (Table 4.3). The optimization results are shown in Figure 4.4.

No holes:	On	Off
Weight [kg]:	3.73	5.13
Element size [mm]:	3	3

No holes:	On	Off
Weight [kg]:	4.95	7.40
Element size [mm]:	6	6

Table 4.3: Weight difference between *no holes* option set to On or Off.

In this case the weight difference between the different *no holes* options also seems to be mesh size dependent. The weight increase is 1.40 kg and 2.45 kg for an element size of 3 mm and 6 mm, respectively.

4.3 One or two design spaces

The purpose of dividing the design space into two design spaces is to illustrate a core, thus to get a cavity in the middle of the casting.

When only a *single* draw direction is used on each design space, as shown in Figure 4.5, the outer boundary keeps the same shape as the design space. Therefore *split* draw direction should be used on both design spaces (Figure 4.6) to get a suitable design.

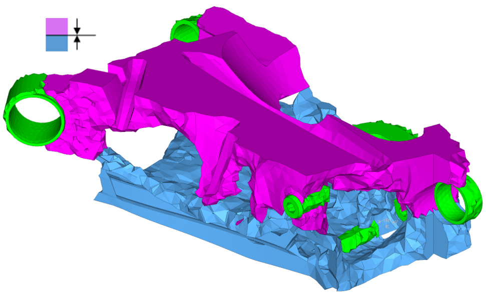

Figure 4.5: Optimization result where *single* draw direction has been applied on the upper and the lower design space.

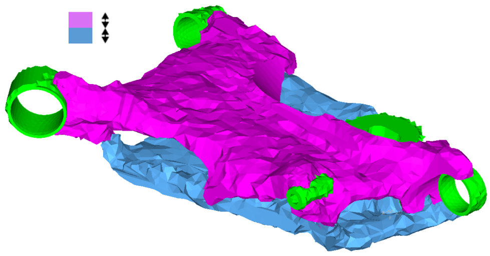

Figure 4.6: Optimization result where *split* draw direction has been applied on the upper and the lower design space.

The parting line between the upper and lower design space is selected manually without any particular preferences. Preferably this parting line should be optimized somehow which are further discussed in Section 8.

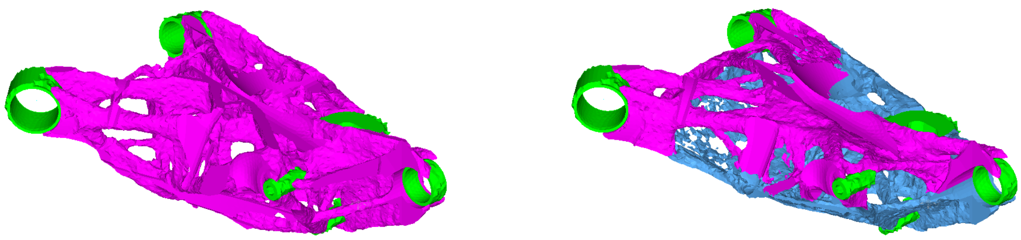

Figure 4.7: One design space (left) compared with the use of two design spaces (right).

As presented in Table 4.4 the optimization using two design spaces becomes lighter compared to when only using one design space. The optimization using two design spaces has a *split* draw direction applied on both the upper and the lower design space (Figure 4.3).

One issue occurred when two design spaces were used. As can be seen in Figure 4.8 the ribs does not cohere properly and the ribs always tend to turn 90 degrees to the free surface of the design space.

	1 Design Space	2 Design Spaces
Weight [kg]:	5.215	5.048
Element size [mm]:	6	6
No holes:	Off	Off
Draw:	Split	Split x 2

Table 4.4: Weight difference between using one compared to two design spaces.

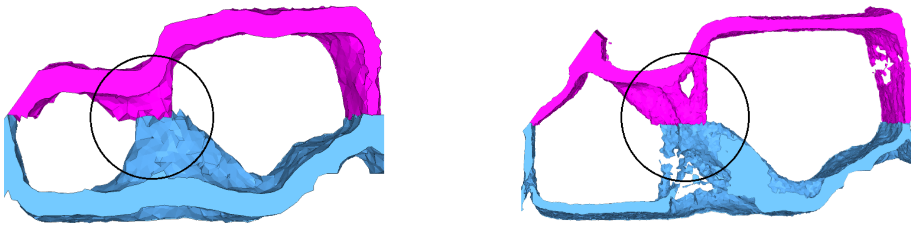

Figure 4.8: Picture of an issue that occurred when two design spaces were used. Same error shown for a coarse mesh (left) and finer mesh (right).

4.4 MINDIM - Member size control

The member size control MINDIM has to be set to a value within an interval based on the element size (described in Subsection 3.1.4). For an element size of 3 mm the total number of elements becomes $N = 8,320,344$. The total volume of the design space is $1.50 * 10^7$ mm^3. Average element size can then be calculated as:

$$\bar{x} = \frac{\sqrt[3]{V_{tot}}}{N} = \frac{\sqrt[3]{1.5 * 10^7}}{8,320,344} = 1.8 \tag{4.1}$$

$$3 * \bar{x} < MINDIM < 12 * \bar{x} \tag{4.2}$$

$$3.65 < MINDIM < 14.60 \tag{4.3}$$

As shown in Table 4.5, a larger MINDIM value results in a heavier optimization design. Pictures of the optimized design with different MINDIM values are shown in Figure 4.9.

MINDIM [mm]:	5	9	12
Weight [kg]:	3.04	3.94	4.06
TOPDISC:	On	On	On
Element size [mm]:	3	3	3

Table 4.5: Weight difference between different member sizes. No draw directions are used and only one design space is used in all three cases.

It can also be seen in Table 4.6 that the topology optimization using MINDIM 5 mm gives a lighter result compared to the unconstrained topology optimization. Nevertheless, it can not be considered as a generic outcome that the implementation of a MINDIM 5 mm always results in a lower mass compared to the unconstrained topology optimization (further discussed in Chapter 8).

As mentioned in Subsection 3.1.4, members slightly smaller than the specified MINDIM value can occur if these members are very important for the load transmission. This

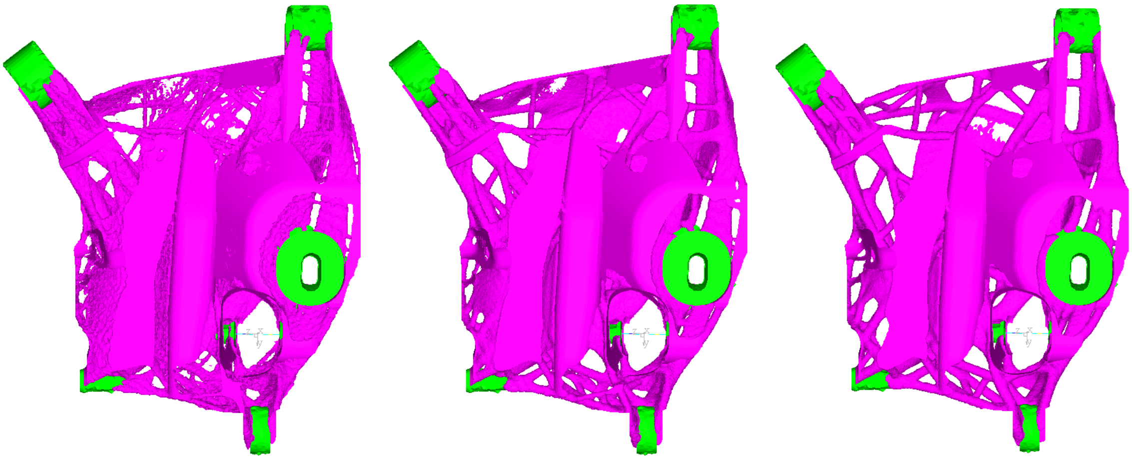

MINDIM = 5 mm MINDIM = 9 mm MINDIM = 12 mm

Figure 4.9: Pictures of the optimized design with three different MINDIM values.

	Unconstrained	MINDIM 5 mm
TOPDISC:	Off	On
Weight [kg]:	3.38	3.04

Table 4.6: Weight difference between the unconstrained topology optimization and when using MINDIM 5 mm.

phenomena appears in some of the topology results and are illustrated in Figure 4.10 where the MINDIM was set to 9 mm.

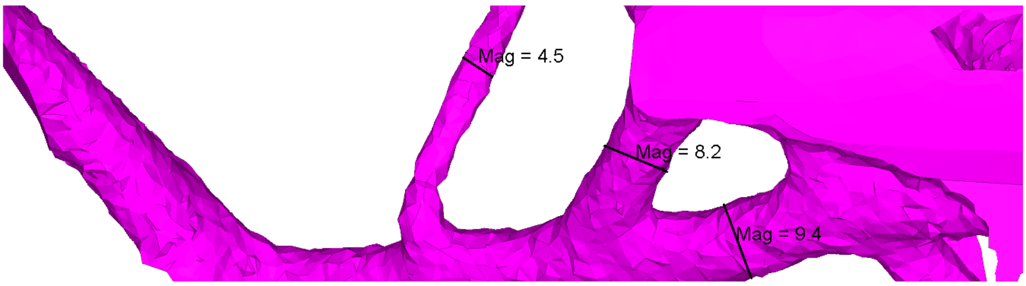

Figure 4.10: Although MINDIM = 9 mm are prescribed, a member with diameter 4.5 mm is still neither removed nor increased in thickness.

This becomes a problem when MINDIM intends to be used to control members due to manufacturing limitations. As mentioned in Section 2.2 it is not possible to cast members with a diameter smaller than 5 mm. If this can not be controlled by MINDIM then some other constraint has to be applied to fulfill this casting requirement. Otherwise these members have to be tracked and modified manually after the topology optimization, which would be very time consuming.

4.5 TOPDISC - Discretization control

By activating TOPDISC, more discrete result i.e. results with less semi-dense elements, is obtained. Two different optimization results combined in the same picture is shown in Figure 4.11. As can be seen in Figure 4.11, the black model with TOPDISC deactivated consists of more spread out element and the elements are not as concentrated to the load transmission paths as the gray model.

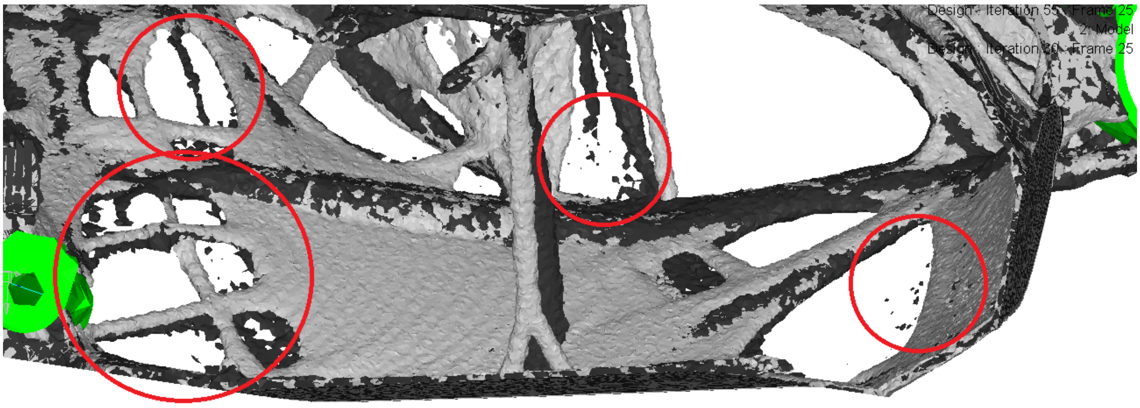

Figure 4.11: Two different optimization results combined in the same picture. Gray: TOPDISC = On. Black: TOPDISC = Off.

As can be seen in Table 4.5 the design becomes slightly lighter when TOPDISC is activated. Nevertheless, this can not be used as a generic conclusion since other topology optimization set-ups with different element size has resulted in the opposite outcome. Maybe this is a matter of element dependence, which could be investigated further. Despite this, TOPDISC is recommended to be used for all topology optimizations using manufacturing constraints since it is preferable to avoid loose and spread out elements.

Split draw, holes & 2DS

TOPDISC:	On	Off
Element size [mm]:	3	3
Weight [kg]:	3.69	3.73

Table 4.7: Weight difference between TOPDISC On and Off.

4.6 Summary

It is recommended to always begin with running an unconstrained topology optimization. This result should mainly be used as a reference and should be analyzed to see which kind of structure the optimization is aiming for. Thereafter, the prioritized optimizations to run are the one using only member size control and the one with two design spaces with *split* draw direction. Due to the fact that they gave the results with the lowest masses when the different manufacturing settings were investigated. Moreover, if the unconstrained result takes the form as a shell structure it is particularly recommended to run an optimization using *split* draw directions on two design spaces.

The *no holes* option should always be inactivated. Even though the implementation of a MINDIM 5 mm not necessarily results in a lower mass, this option should always be used due to a manufacturing point of view, since it is not possible to cast sections in aluminum thinner than 5 mm (Section 2.2). From a modeling and a manufacturing point of view it is preferable to get a geometry with less loose and spread out elements. From both a structural strength and manufacturing point of view it is also preferable to get elements concentrated to the load transmission paths. Therefore, the TOPDISC is recommended to be activated in all topology optimizations using manufacturing constraints, even though it necessarily not contributes to a lower mass.

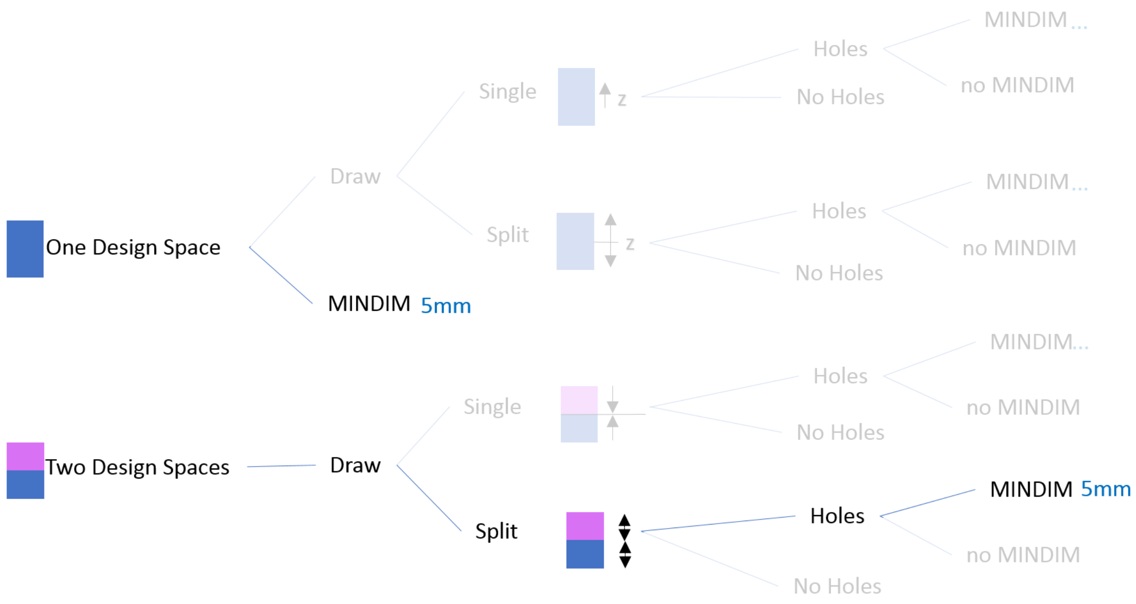

Figure 4.12: Manufacturing constraints eliminated from a weight perspective. The two lightest manufacturing constraint set-ups are highlighted.

Figure 4.12 shows the manufacturing constraint set-ups that are eliminated in this section. The three results with the lowest mass are presented in Table 4.8. The fact that the topology result MINDIM 5 mm (A) actually becomes lighter than the unconstrained topology optimization (B) are further discussed in Section 8.1, but it can be mentioned that the results looks very similar. The topology results B and C are further investigated and compared from a casting point of view in Section 6.2.

A	MINDIM 5 mm	TOPDISC: On	3.04 kg
B	Unconstrained	TOPDISC: Off	3.38 kg
C	2DS, split draw, no holes, MINDIM 5 mm	TOPDISC: On	3.90 kg

Table 4.8: The weight of the three lightest topology optimization results.

5| Results
Topology result into C2C

As mentioned in Subsection 3.1.6, the topology optimization result are possible to post process and export in several different ways. Pros and cons using the post processing tools OSSmooth, iso averaging method and Shrink Wrap are presented in this chapter.

Some general problems occurred when post processing the topology results. For example, the main part of the topology results contained a lot of spread out and loose element. This becomes a problem, partly because these elements will not contribute to the structural strength. These will instead contribute to a higher mass. Furthermore, these loose elements will cause problem in the casting simulation. Completely loose elements can be removed relatively simple with some manual procedures. All elements which are not connected to the main geometry can be removed by selecting the elements to be preserved using "attached elements", then reverse the selection and delete these elements. But the problem is only partly solved using this method. Still, elements that are slightly attached to the main geometry will remain, as illustrated in Figure 5.1. It would be possible to remove these elements manually but this is not an optimal solution since the required manual work would be very time consuming for a large range of design concepts.

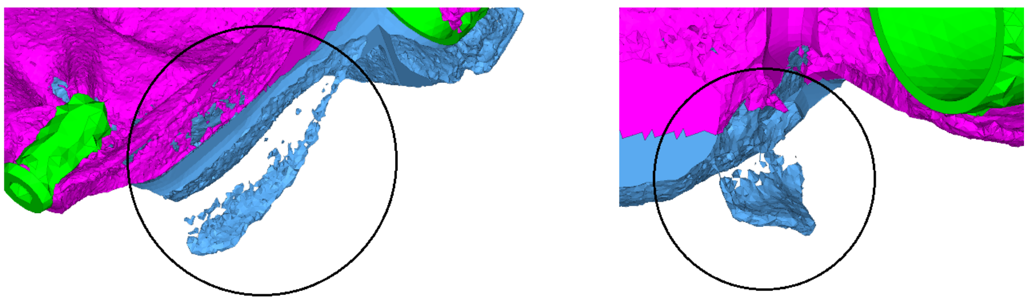

Figure 5.1: Post processing problems. Loose parts in the optimization result.

The fastest and most simple way is to export an iso-surface directly from HyperView as an .stl file. This iso-surface can be treated with an averaging-method before the export from HyperView. An iso surface without any averaging method will result in a relatively rougher surface compared to when an averaging method is applied, as can be seen in Figure 5.2. The averaged iso surface can be then be exported as a .stl file, but the problem occurs when the averaged iso surface is imported into C2C. C2C gets problem since the iso surface is not properly connected to form an enclosed single body volume which the C2C requires. A similar iso surface is achieved with the OSSmooth tool using the *geometry* option, illustrated in Figure 5.4. The OSSmooth option *ReAnalysis* on the other hand generates a volume mesh but problems occurred due to the same issue, i.e. that the iso surface did not form an enclosed volume. The advantages with the OSSmooth *ReAnalysis* is that it maintains the connectivity to the loads and can be re-analyzed. But in this case, it is still necessary to break the connectivity anyhow, since the design space and the non design space will be re-modelled into one enclosed single volume surface mesh.

By importing the averaged iso-surface from HyperView into HyperMesh the Shrink Wrap is applied to this surface to get an enclosed volume with an even smoother surface. Figure

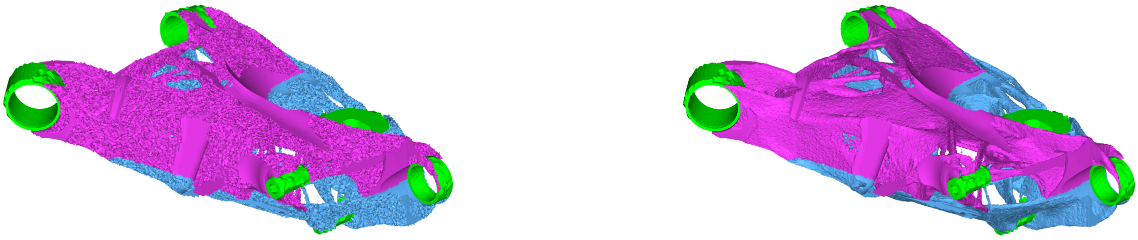

a) None Averaging Method. b) Simple Averaging Method.

Figure 5.2: None averaging method versus simple averaging method.

5.3 shows how Shrink Wrap surface (orange) of the averaged iso-surface (red) enlarge the total volume of the design (Table 5.1). The Shrink Wrap combinations and options, which results in the lowest volume increase are the *loose* Shrink Wrap with an element size of 1 mm.

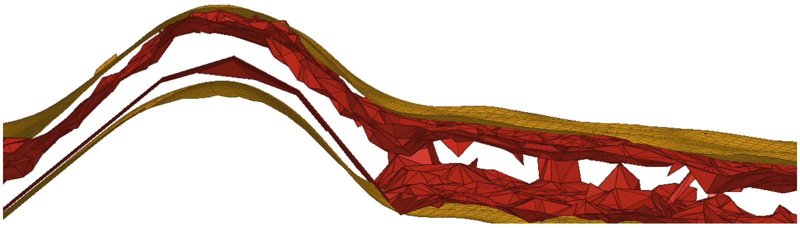

Figure 5.3: Picture showing the thickness increase when using Shrink Wrap.

		Weight [-]
Averaging iso-surface	Red	1
SW* on the averaged iso-surface	Orange	1.4

**loose* Shrink Wrap with element size 1 mm.

Table 5.1: Mass increase when using Shrink Wrap.

The Shrink Wrap surface are constructed by quad elements, therefore all elements are required to be split into trias in order to export a proper .stl file.

The volume elements from the .TCL file can also be used for post processing. The surface gets the same finish as the iso-surface without averaging method, shown in Figure 5.2. To transform this very coarse volume mesh into a smooth surface, a very loose wrap has to be performed which further will results in a large volume decrease. Therefore, the TCL volume elements are not recommended to be used for this purpose. Figure 5.4 shows the wall thickness difference of the TCL volume mesh and the averaged iso-surface. This wall thickness will be mesh dependent and will decrease with decreased element size.

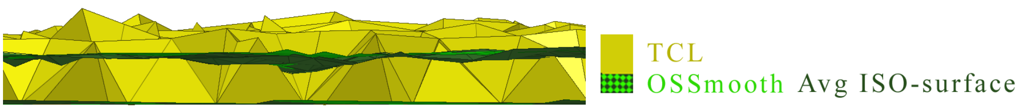

Figure 5.4: Thickness difference of the TCL volume elements and averaged iso-surface.

The enlarged geometry generated using Shrink Wrap, which are used for the casting simulations, are not intended to be used as the reference model for the CAD realization in the end of the development process. The CAD realization should instead be based on the initial topology optimization result.

5.1 Summary

The least volume enlarging, less time consuming and most robust way to get the topology result into the casting simulation turned out to be by generating an smooth and enclosed surface mesh, based on an averaged iso surface of the topology optimization result, using the Shrink Wrap tool with the *loose* option and an element size of 1 mm.

6| Results
Methods to evaluate castability

Different methods of how to measure castability is presented in this chapter. Firstly, different approaches are investigated and evaluated using the Optimized Design and Current RLCA (Section 6.1). Secondly, the established castability evaluation procedure is applied on two different topology optimization results (Section 6.2).

6.1 Castability evaluation of the Optimized Design and Current RLCA

To get a better understanding of which conclusions that can be drawn from the simulation results, it was decided to begin with comparing the Optimized Design with the Current RLCA, since it was already known that the Optimized Design was not feasible to cast. This was expected to be confirmed by using C2C.

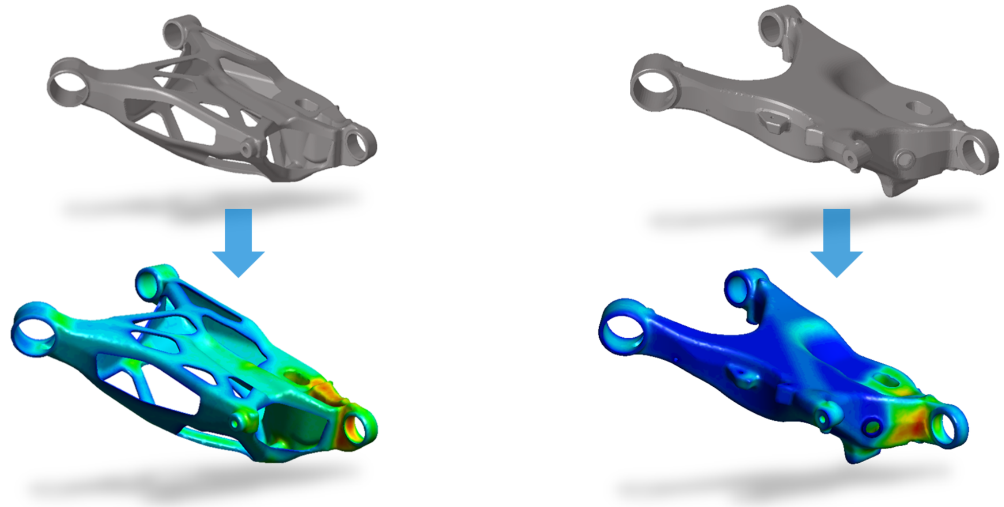

Figure 6.1: Illustrating picture of the Optimized Design and Current RLCA.

	Optimized Design	Current RLCA
Max Temperature [^{o}C]	365.06	351.97
Max Solidification Modulus [cm]	1.09	1.35
Min Solidification Modulus [cm]	0.20	0.36
Max Niyama [(^{o}C*s)$^{0.5}$/mm]	4.47	5.08
Min Niyama [(^{o}C*s)$^{0.5}$/mm]	0.0010	0.0015
Max Macro Porosity [mm^3]	2 015	6 635
Solidification Time [s]	13.42	20.56

Table 6.1: C2C solidification simulation results of the Optimized Design and the Current RLCA.

The maximum and minimum results from C2C for the Optimized Design and the Current RLCA are presented in Table 6.1. However, the maximum or minimum values of neither temperature, solidification modulus nor Niyama values can be directly related to castability. As for the solidification modulus, it is about in which direction and how it changes over the structure that affects the castability. Max macro porosity shows that the Current RLCA gets the largest porosity volume compare to the Optimized Design. The porosity percentage and liquid fraction results are not included in Table 6.1 since they are only presented as pictures and animations in C2C. All C2C input parameters as well as the contour plot results are presented in Appendix A and B, respectively. By only analyzing the values, contour plots and animations in C2C, the Optimized Design seemed to have a better castability, apart from when looking at the liquid fraction (see Subsection 6.1.3). By post-processing and analyzing the values in HyperView and Compose, additional results could be captured.

Moreover, it is of importance to remember that no consideration is taken to the filling process. The solidification simulation starts with a perfectly filled component, i.e. problems during the filling will not be captured in the solidification simulation. Since the Optimized Design consists of very thin members in relation to the length of each member, problem will probably occur when trying to fill the part.

	Optimized Design	Current RLCA
Total number of nodes	1 182 621	1 549 536
V_c [m^3]	$1.16 * 10^{-3}$	$1.51 * 10^{-3}$
V_a [m^2]	$4.58 * 10^{-1}$	$4.80 * 10^{-1}$

Table 6.2: General data for the Optimized Design and the Current RLCA.

6.1.1 Niyama

The plots in Figure 6.2 displays all values below 0.3 which represents the critical values (described in Subsection 2.2.3). As can be seen in Table 6.3 the Current RLCA consists of more critical nodes compared to the Optimized Design, but on the other hand it represents a smaller amount of nodes in relation to the total amount of nodes.

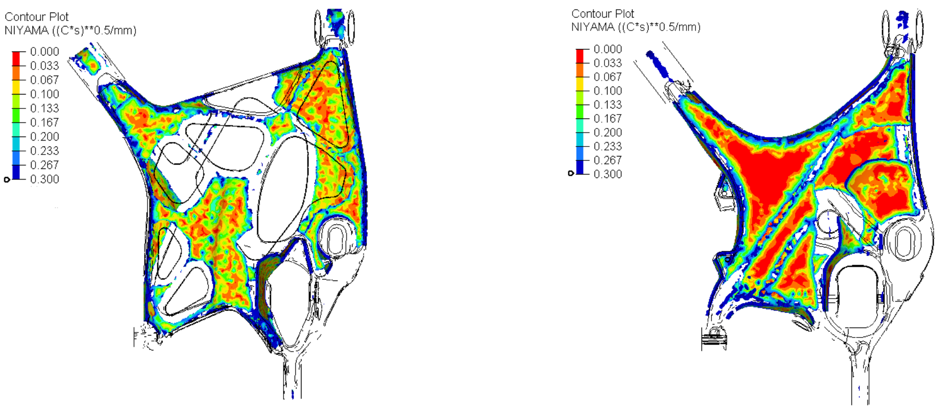

Figure 6.2: Plot of the critical Niyama regions, i.e. where the Niyama value ≤ 0.3.

	Optimized Design	Current RLCA
Niyama ≤ 0.3	64 565	70 476
	5.46%	4.55%

Table 6.3: Number of critical Niyama nodes.

6.1.2 Porosity

Porosity results are only calculated for the final time step in the solidification simulation. The post processed porosity results (Table 6.4) generated in Compose shows that the Current RLCA contains more critical nodes with respect to porosity [%] but contains a slightly lower porosity volume [mm^3] when the total amount of nodes is taken into account.

An arbitrary critical threshold value of 100 mm^3 is used for the porosity volume. A critical threshold value of 20% was picked, based on recommendations from casting experts at Volvo Cars. The same threshold values were also used in the HotSpots tool.

It was discovered that the amount of hot spots depends on the searching diameter distance, as shown in Table 6.4. Therefore, the hot spots results are not further used due to the inconsistency caused by the searching distance dependence, which very likely can lead to inaccurate and misleading results.

	Optimized Design	Current RLCA
Porosity ≥ 100 mm^3	932	1 195
	0.78‰	0.77‰
Hot spots th = 100 mm^3, d = 0.02 m	11	10
Hot spots th = 100 mm^3, d = 0.05 m	10	10
Hot spots th = 100 mm^3, d = 0.10 m	8	7
Porosity ≥ 20%	17 853	33 673
	1.5%	2.2%
Hot spots th = 20%, d = 0.05 m	13	13

Table 6.4: Number of critical porosity nodes and number of hot spots.

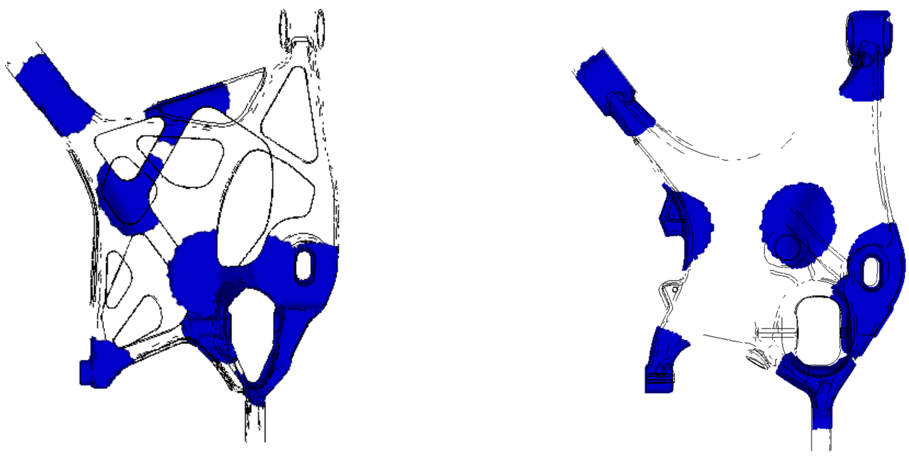

Optimized Design　　　Current RLCA

Figure 6.3: Plot of the porosity hot spots captured with the HotSpots tool (th = 100 mm^3 and d = 0.05 m).

6.1.3 Liquid fraction

The liquid fraction of the Optimized Design (at t = 3.68 s) and the Current RLCA (at t = 4.13 s) are presented in Figure 6.4. By looking at the animations of the liquid fraction it can be seen that the Current RLCA has a directional solidification that reduces the occurrence of hot spots, meanwhile the Optimized Design get several hot spots located at very disadvantageous areas, where it is quite inconvenient and unsuitable to place feeders. These critical hot spots are marked in Figure 6.4.

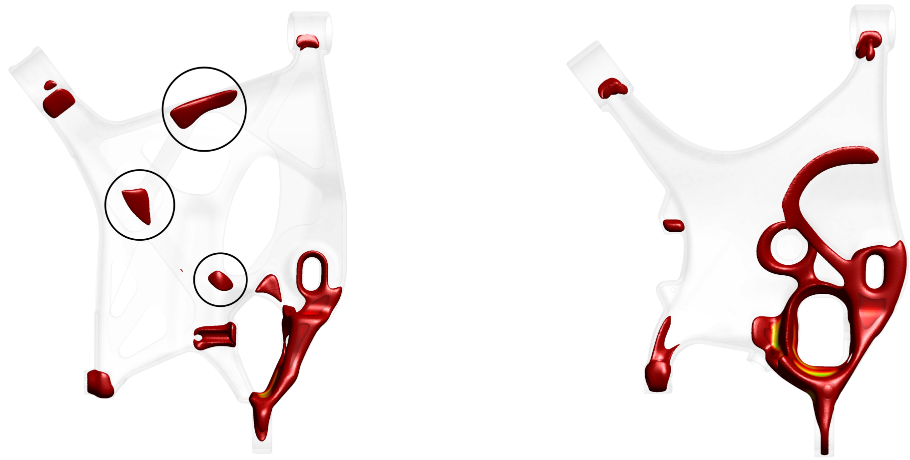

Optimized Design
t = 3.68 s

Current RLCA
t = 4.13 s

Figure 6.4: Liquid fraction of the Optimized Design and the Current RLCA.

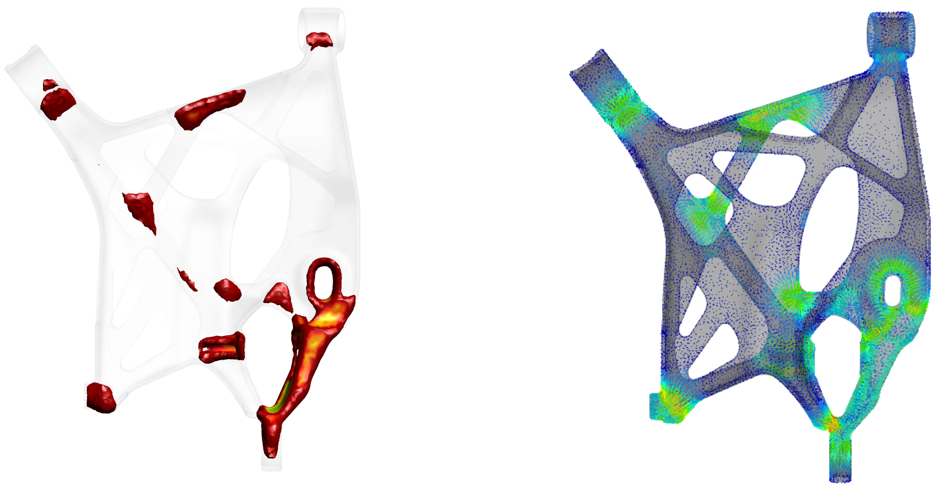

Optimized Design
Liquid fraction

Optimized Design
Temperature gradients

Figure 6.5: Plots of how the Liquid fraction correlates to the temperature gradients.

6.1.4 Temperature gradients

The liquid fraction hot spots can be captured and counted by using the HotSpots tool on the temperature gradients, at a certain time step $t_{3.68}$ (Figure 6.6). In Figure 6.6 the threshold $G_{crit} = 9$ ^{o}C/mm were used in combination with a diameter of 0.02 m.
The problem is that the temperature gradients are computed for nearly 100 time steps, meanwhile the hot spots occurs in different time steps i.e. at different solidification time both within the same model and among different models. There is no general rule that can tell when the liquid fraction hot spots occurs during the solidification.

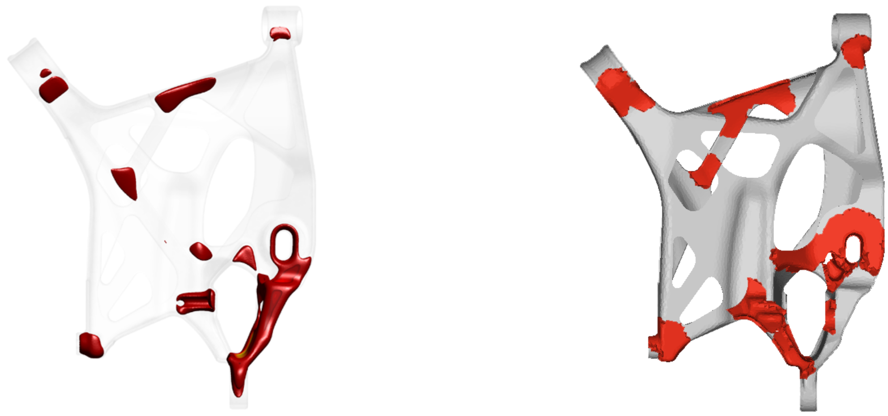

a) Liquid fraction at t = 3.68 s

b) HotSpots of the temperature gradients G ≥ 15 ^{o}C/mm at t = 3.68 s

Figure 6.6: Liquid fraction and temperature gradient hot spots of the Optimized Design.

Another problem that occurred when trying to analyze the temperature gradients numerically was the excessively time-consuming processes when trying to export and work with this large amount of data, i.e. about 15 million values. Therefore, the enveloped temperature gradient results were used instead. No hot spots were visualized in the enveloped temperature gradient contour plot for all time steps. Due to the fact that the highest temperature gradients occur at all wall boundaries in the beginning of the solidification. By excluding the first time steps in the Envelope of the temperature gradients, the hot spots appears in the contour plot and are possible to track using the HotSpots tool.

By examining in how many nodes the temperature gradient exceeds a critical value G_{crit}, it could be seen that the Current RLCA contained less critical temperature gradient nodes compared to the Optimized Design (Table 6.5). Where G_{crit} have been set to an arbitrary value of G_{crit} = 15 ^{o}C/mm.

	Optimized Design	Current RLCA
Max G	31.7	25
Mean G_{env}	11.86	11.66
G ≥ G_{crit}	300 368	374 977
	25.4%	24.2%

Table 6.5: Number of critical temperature gradient nodes.

Furthermore, one additional aspect should be considered. High temperature gradients do not necessarily results in hot spots specifically. It seems like temperature gradients can be relatively high locally, but as long as they are directed against a heat source they will not lead to isolated liquid pools, i.e. hot spots. Hence, the direction of the temperature gradients most likely could tell where a hot spot will arise, as illustrated in Figure 6.7. One hypothesis is that the hot spots can be captured by tracking the directional change of the temperature gradient by calculating the gradient of each (x,y,z) component of the temperature gradient. This is unfortunately not further investigated in this project due to time limitations.

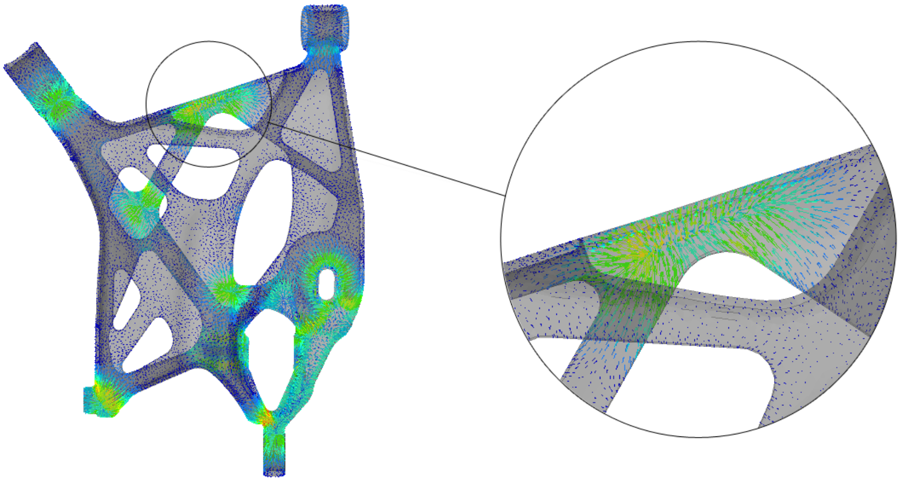

Figure 6.7: Zoomed picture of the temperature gradient vectors and its direction.

Furthermore, the mean value of the temperature gradient, for all time steps, were calculated. The temperature gradient has also been divided into intervals presented in Table 6.6. These calculations were done for the models containing only 29,933 and 41,263 nodes, respectively. It is shown in Table 6.6 that the Optimized Design gets a slightly smaller mean value, compared to the Current RLCA. Meanwhile, it contains more nodes in the top range compared to the Current RLCA.

TempGrad [°C/mm]	0-5	5-10	10-15	15-20	20-25	Max	Mean
Optimized Design	2 352 225	520 005	30 224	1 317	47	24	2.50
	81%	17.9%	1%	0.45%	0.016%		
Current RLCA	3 236 621	755 973	50 921	687	0	19.7	2.51
	80%	18%	1.3%	0.17%	0%		

Table 6.6: Intervals of the temperature gradients, G, of the Optimized Design and the Current RLCA (with less nodes).

6.1.5 Stress mapping

This subsection presents results regarding how Niyama, porosity and temperature gradient results correlates to the stresses over the structure.

To begin with, ordinary linear static strength analysis are performed and shows that the optimized component gets larger (Von Mises) stress levels compared to the Current RLCA. Contour plots of the Enveloped Von Mises stresses are presented in Figure 6.8. In Table 6.7 it can also be seen that the Current RLCA contains less nodes exceeding the arbitrary stress limit of $0.35\sigma_y$.

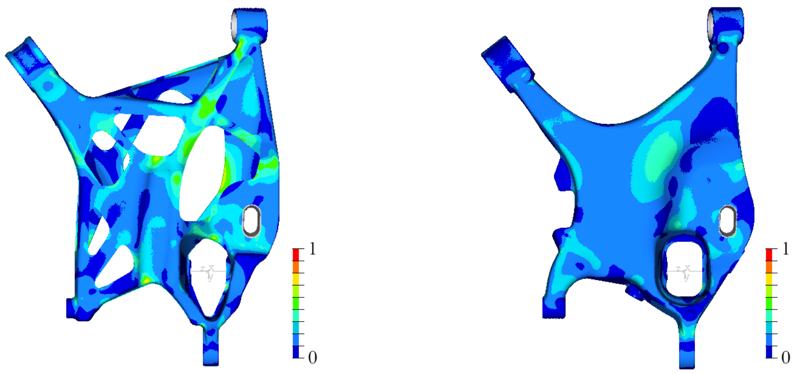

Figure 6.8: Contour plots of normalized Von Mises envelope stresses of the Optimized Design (left) and the Current RLCA (right).

	Optimized Design	Current RLCA
σ_{max}	σ	0.74σ
$\sigma_{env} \leq 0.35\sigma_y$	21 011	495
	1.78%	0.032%

Table 6.7: Stress results of the Optimized Design and the current RLCA.

6.1.5.1 Stresses mapped against Niyama

The Niyama values less and equal to 0.3 are mapped to stresses exceeding 0.35σ. The coinciding nodes i.e. the critical nodes, are circled and presented in red on the right hand side in Figure 6.9.It can be seen in Table 6.8 that the Optimized Design only contains 270 critical nodes and that the Current RLCA does not contains any critical nodes at all.

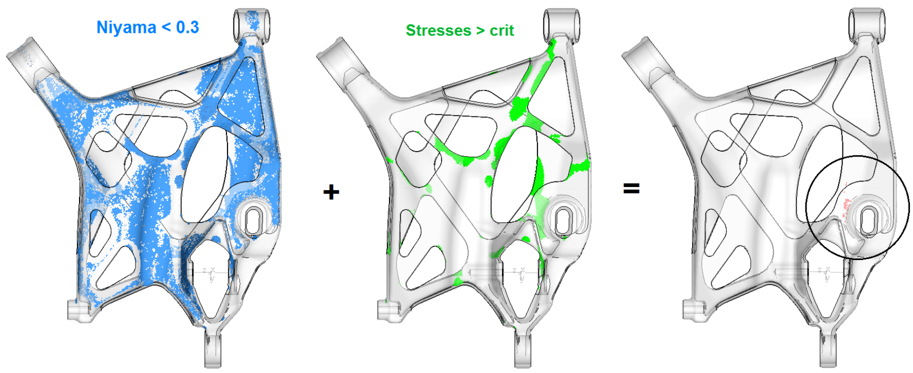

Figure 6.9: The Niyama values less and equal to 0.3 (blue) mapped against stresses exceeding 0.35σ (green) give critical nodes presented in red.

	Optimized Design	Current RLCA
Niyama ≤ 0.3 & $\sigma \geq 0.35\sigma$	270	0
	0.0228‰	0‰

Table 6.8: Number of critical nodes of the Niyama and stress mapping.

6.1.5.2 Stresses mapped against Porosity

Porosity volume greater than 20% and porosity values greater than 100 mm^3 are mapped against stresses exceeding 0.35σ. It can be seen in Table 6.9 that the Optimized Design only contains 4 critical nodes for the porosity [%] and that the Current RLCA does not contains any critical nodes at all. Regarding the porosity volume, none of the designs contain any critical nodes.

	Optimized Design	Current RLCA
Porosity $\geq 20\%$ & $\sigma \geq 0.35\sigma_y$	4	0
	0.0034‰	0‰
Porosity $\geq 100\ mm^3$ & $\sigma \geq 0.35\sigma_y$	0	0
	0%	0%

Table 6.9: Number of critical nodes of the porosity mapped against stresses.

6.1.5.3 Stresses mapped against Temperature Gradients

Temperature gradients greater than $G_{crit} = 15\ ^o$C/mm are mapped against stresses exceeding 0.35σ and are presented in red in Figure 6.10. It can be seen in Table 6.10 that the Optimized Design contains a much larger amount of critical nodes compared to the Current RLCA.

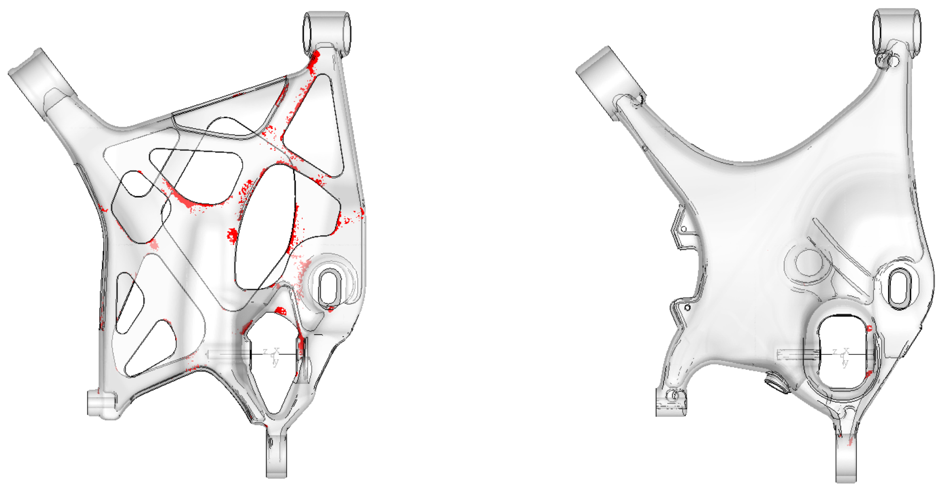

a) Optimized Design　　b) Current RLCA

Figure 6.10: Critical areas when mapping critical temperature gradients against critical stresses.

	Optimized Design	Current RLCA
$G \geq G_{crit}$ & $\sigma \geq 0.35\sigma_y$	9 843	421
	8.323‰	0.27‰

Table 6.10: Number of critical nodes of the temperature gradients mapped to stresses.

6.1.6 Summary of castability analysis of Optimized Design and Current RLCA

This section presents the evaluation results for the Optimized Design and the Current RLCA, by applying the weighting methods presented in Section 3.4 on the results from Section 6.1. The results from Section 3.4 constitute the criteria presented in Table 6.11, which furthermore is used to determine the weighted value W_j. The weighted values W_j are normalized according to equation (3.4) which contributes to the rating values R_j and R_j^* ((3.5) and (3.7)), for each design concept j. The lower the value the better properties of the design. The castability criteria c_3 (described in Subsection 2.2.2) is not included in these evaluations since there is no trivial way of counting the number of features in a design.

			Optimized Design	Current RLCA
	K1	Mass [kg]	3.15	4.07
	K2	σ_{max}	σ	0.74σ
	K3	$\sigma \geq 0.35\sigma_y$	1.78%	0.032%
	K4	V_b/V_c	12.5	10
	K5	$A_c/(6 * V_c^{2/3})$	7.14	6.25
Niyama	K6	Niyama ≤ 0.3	5.46%	4.55%
Porosity	K7	Porosity $\geq 20\%$	1.5%	2.2%
	K8	Max Porosity [mm^3]	2 015	6 635
	K9	Porosity ≥ 100 mm^3	0.78%	0.79%
Temperature Gradients	K10	G_{max}	31.5	25
	K11	G $\geq$ G_{crit}	25.4%	24.2%
Stress mapping	K12	Niyama ≤ 0.3 & $\sigma \geq 0.35\sigma_y$	0.0228‰	0‰
	K13	G $\geq$ G_{crit} & $\sigma \geq 0.35\sigma_y$	8.323‰	0.27‰
	K14	Porosity $\geq 20\%$ & $\sigma \geq 0.35\sigma_y$	0.0034‰	0‰
	K15	Porosity ≥ 100 mm^3 & $\sigma \geq 0.35\sigma_y$	0%	0%

Table 6.11: All results of the Optimized Design and the Current RLCA.

The weighted results are presented in Table 6.12. The rating value R_{K4-K16} has been introduced to define the castability rating separately. Meanwhile R_{K1-K3} are based on the additional properties alone. The rating values presented in Table 6.13 shows that the Current RLCA gets a lower, i.e. better, rating compared to the Optimized Design, even when the weight is considered as equally important as the rest of the criteria together.

	Optimized Design	Current RLCA
K1	0.77	1
K2	1	0.74
K3	1	0.018
R$_{K1-K3}$	1	0.89
K4	1	0.77
K5	1	0.88
K6	1	0.83
K7	0.68	1
K8	0.3	1
K9	1	0.99
K10	1	0.79
K11	1	0.95
K13	1	0
K14	1	0.03
K15	1	0
K16	0	0
R$_{K4-K16}$	1	0.73

Table 6.12: Weighted values of the Optimized Design and the Current RLCA.

	Optimized Design	Current RLCA
R_j	1	0.71
R_j^*	1	0.94

Table 6.13: Rating values of the Optimized Design and the Current RLCA.

6.2 Evaluation of design concept B and C

The previously selected design concepts B and C (Chapter 4) are in this section further investigated with respect to castability. The results are presented in Table 6.15.

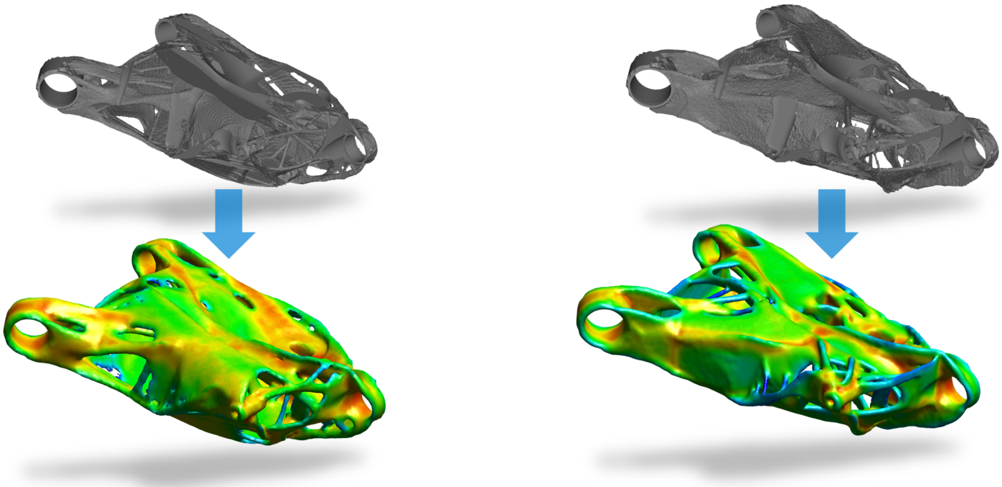

Figure 6.11: Illustrative picture of the design concepts B and C.

	B	C
Total number of nodes	176 822	175 243
V_c [m^3]	$2.66 * 10^{-3}$	$2.75 * 10^{-3}$
V_a [m^2]	$7.24 * 10^{-1}$	$6.98 * 10^{-1}$

Table 6.14: General data of the design concepts B and C.

Since the volume expansion (described in Chapter 5) results in thicker members, the element size of 3 mm could be used which resulted in around 170,000 total number of nodes (Table 6.14).

Regarding the design concepts B and C, their actual mass in the strength and casting simulations are about 1.4 times larger than the mass of the topology optimized design (Table 6.15). This, due to the volume increase described in Chapter 5. The enlarged volume yields a much higher structural strength which further results in significantly low stress levels in the structure. Number of nodes exceeding the critical stress was 19 and 21 for the design concepts B and C, respectively. The critical stress value of $\sigma_{crit} \geq 100$ MPa was shown no longer relevant to use for the stress mapping, since it only returned zeros. Therefore, the critical stress was changed to $\sigma_{crit} \geq 25$ MPa. The amount of nodes exceeding $\sigma_{crit} \geq 25$ MPa now became 72,419 and 71,249, respectively.

The weighted values are presented in Table 6.16. Since draw direction is beneficial for the castability, it also should be considered in the evaluation. Therefore, criteria *K16* is added and represents draw direction manufacturing constraint. $K16 = 0$ indicate that draw direction has been activated (1.0 = deactivated). In table 6.17 it is shown that both of the rating methods consider the design concept C better than design compared B.

			B	C
	K1	Mass [kg]	3.38	3.9
	K2	σ_{max}	σ	0.76σ
	K3	$\sigma \geq 100$ MPa	0.11‰	0.12‰
	K4	V_b/V_c	5.62	5.43
	K5	$A_c/(6 * V_c^{2/3})$	6.29	5.92
Niyama	K6	Niyama ≤ 0.3	4.52%	3.54%
	K7	Porosity ≥ 20%	0.677%	0.750%
Porosity	K8	Max Porosity [mm^3]	657.3	892.7
	K9	Porosity ≥ 100 mm^3	0.62‰	0.66‰
Temperature	K10	G_{max}	40.24	29.34
Gradients	K11	$G \geq G_{crit}$	6.35 %	4.91 %
	K12	Niyama ≤ 0.3 & $\sigma \geq 25$ MPa	8.79‰	6.47‰
Stress	K13	$G \geq G_{crit}$ & $\sigma \geq 25$ MPa	3.62%	2.83 %
mapping	K14	Porosity ≥ 20% & $\sigma \geq 25$ MPa	2.25 ‰	2.53 ‰
	K15	Porosity ≥ 100 mm^3 & $\sigma \geq 25$ MPa	0.16 ‰	0.25 ‰

Table 6.15: All results of the design concepts B and C.

	B	C
K1	0.86	1
K2	1	0.76
K3	0.89	1
R_{K1-K3}	1	0.998
K4	1	0.97
K5	1	0.94
K6	1	0.78
K7	0.90	1
K8	0.74	1
K9	0.93	1
K10	1	0.73
K11	1	0.77
K12	1	0.74
K13	1	0.78
K14	0.89	1
K15	0	0
K16	1	0
R_{K4-K16}	1	0.85

Table 6.16: Weighted values of the design concepts B and C.

	B	C
R_j	1	0.877
R_j^*	1	0.996

Table 6.17: Rating values of the design concepts B and C.

6.3 Summary

Topology optimization results can be compared and evaluated, to eliminate the less suitable designs from a casting point of view, by weighting casting properties, weight and strength properties together. Several evaluation criteria are considered with the aim to evaluate castability as accurate as possible. In addition to mass, max porosity and max stress, the following criteria values can be generated:

- Niyama:
  Niyama ≤ 0.3
- Porosity:
  Porosity $\geq 20\%$
  Porosity $\geq$ Porosity$_{crit}$
- Temperature Gradients:
  G_{max}
  $G \geq G_{crit}$
- Stress mapping:
  $\sigma \geq \sigma_{crit}$ & Niyama ≤ 0.3
  $\sigma \geq \sigma_{crit}$ & $G \geq G_{crit}$
  $\sigma \geq \sigma_{crit}$ & Porosity $\geq 10\%$
  $\sigma \geq \sigma_{crit}$ & Porosity ≥ 100 mm^3

Since there is no general rules to define the critical threshold values for neither the porosity, temperature gradient or stresses in combination with casting defects, arbitrary values are used. Yet, it is important that the threshold values are the same for the design concepts to be compared. Thus, a design concept can not be rated separately but only graded in relation to other design concepts.

Results generated using the HotSpots tool was decided to not be used due to the inconsistency caused by the searching distance dependence which can cause inaccurate and misleading results.

7| Development process of topology optimized casted components

This master thesis has resulted in a suggested development process for topology optimized casted components, presented in this chapter. Figure 7.1 shows a schematic flowchart of the overall working procedure and are further described in the numbered list below.

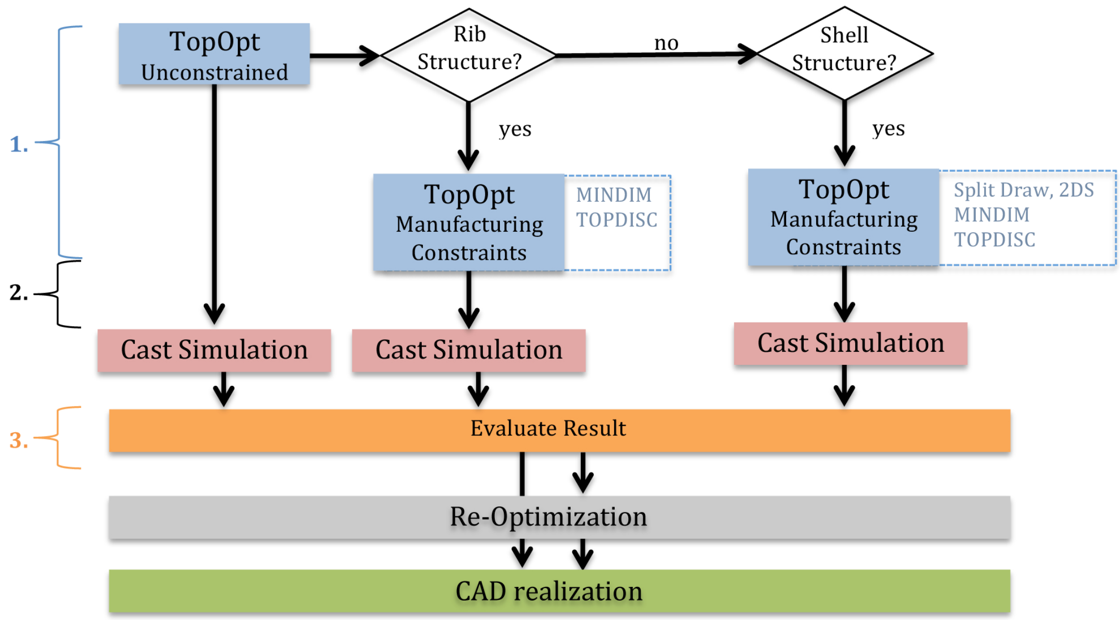

Figure 7.1: Schematic flowchart of the development process of topology optimized casted components.

1. **Topology Optimization:**
   An unconstrained topology optimization should first be generated, mainly to be used as a reference. The unconstrained topology optimization result can be analyzed to see which kind of structure the optimization is aiming for when no manufacturing constraints are applied. Thereafter, the prioritized optimizations to run are the one using only member size control and the one with two design spaces with *split* draw direction. Particularly if the unconstrained result takes the form as a shell structure, it is recommended to run an optimization using *split* draw directions on two design spaces. As presented in Section 4.6 the *no holes* option should always be inactivated. TOPDISC is recommended to be activated for all optimizations using manufacturing constraints and MINDIM 5 mm should always be used for castings in aluminum.

2. **Topology result into casting simulation:**
   As presented in Chapter 5 the least volume enlarging and most robust and time efficient way to get the topology result into the casting simulation, is to generate a smooth and enclosed surface mesh, based on an averaged iso surface of the topology optimization result, using the Shrink Wrap tool with the *loose* option and an element size of 1 mm. The Shrink Wrap surface mesh consists of quad elements which should be split into triangular elements. The surface can thereafter be exported as a .stl file which furthermore can be imported into the casting simulation software.

3. **Evaluate castability:**
As presented in Chapter 6 the castability can be evaluated numerically by post-processing the casting simulation results in HyperView and Compose. In order to produce the stress-mapping results, a mesh convert has to be performed (further described in Section 3.3). The results are thereafter used as criteria values (listed below). The criteria values are normalized according to equation (3.3) and are further used to bring out a rating value for each design concept. Only two simple approaches of how to determine the rating value has been used in this thesis. These are further described in Section 3.4.

Niyama:
Niyama ≤ 0.3

Porosity:
Porosity $\geq 20\%$
Max Porosity [mm^3]
Porosity ≥ 100 mm^3

Temperature gradients:
G_{max}
$G \geq G_{crit}$

Stress mapping:
$\sigma \geq \sigma_{crit}$ & Niyama ≤ 0.3
$\sigma \geq \sigma_{crit}$ & $G \geq G_{crit}$
$\sigma \geq \sigma_{crit}$ & Porosity $\geq 10\%$
$\sigma \geq \sigma_{crit}$ & Porosity ≥ 100 mm^3

Additional properties:
Mass
V_b/V_c
$A_c/(6 * V_c^{2/3})$
σ_{max}
$\sigma \geq \sigma_{crit}$

Since there is no general rules to define the critical threshold values for neither the porosity, temperature gradient or stresses in combination with casting defects, arbitrary values are used. Yet, the threshold values has to be the same for the design concepts to be compared. Thus, a design concept can not be rated separately, but only graded in relation to other design concepts.

Since the geometry generated with the Shrink Wrap tool in HyperMesh (which is used for the castability evaluations) is significantly enlarged, it also will yield much higher structural strength. This has to be taken into account when the critical stress value, used for the stress-mapping, are picked. However, the evaluation presented in this thesis does not replace the ordinary strength analysis. Moreover, the enlarged geometry generated using Shrink Wrap should only be used for the casting evaluation i.e. it is not intended to be used as the reference model for the CAD realization. The CAD realization should instead be based on the initial topology optimization result of the elected design concept.

8| Discussion

This chapter will discuss and interpret the results of this master thesis project.

8.1 Topology Optimization

It was unexpected to see some of the topology optimization results contained loose hanging parts in the structure, since the main objective of the optimization is to reduce unnecessary mass and maximize stiffness. The phenomena displayed in Figure 5.1 might be related to the *no holes* option since it seems to only occur when *no holes* option is activated.

It was observed that e.g. the unconstrained topology optimization results of this RLCA component contains several thin members inside of the structure. This result match the one obtained by Larsson [2]. Though, this thesis is taken into account that advanced cores can be produced using 3D casting. Yet, the shake out process, when the sand is removed from the casting, is not considered. A complex core will probably contribute to a more complicated and time consuming shake out process. Moreover, despite the possible to cast members all the way down to 5 mm in diameter [18], one still has to consider where these thin members are located in the structure. Due to the fact that thin and sensitive parts of the structure should not be placed in the parting line [1], which has not been considered in this project.

It was believed that by activating the *no holes* option, the optimization should give a more deviating structure compared to when the *no holes* option was deactivated. It was thought e.g that the ribs should be rearranged or that the adjacent walls would get a decreased thickness, in order to achieve an optimal structure without any holes. However, it seems like the holes are only filled with additional material and that the structure is not changed any further.

This thesis showed that it is possible to illustrate a core in the casting by dividing the design space into two design spaces and by applying *split* draw direction on each design space. In the previous thesis by Larsson [2] it turned out that *split* draw direction on one design space lead to a too large weight increase, which match the observing in this thesis. But by instead using two design spaces, the weight increase became much smaller. Yet, the placement of the parting line between the upper and lower design space is selected manually and should preferably be optimized somehow. A routine similar to the one used in OptiStruct, which finds the optimal parting line in the draw manufacturing constraint, should be possible to develop in order to find the optimal parting line between two design spaces. Otherwise, one suggestion could be to simply scan the unconstrained topology optimization to identify the z-plane containing the least amount of element (or least dense elements). This z-plane can then be used as the splitting plane between the upper and the lower design space.

A problem occurred when two design spaces were used. As shown in Figure 4.8 the ribs does not cohere properly and the ribs always tend to turn 90 degrees to the free surface of the design space. This phenomenon is hard to explain but could be due to a numerical problem.

It is recommended to find a way to consider or prevent the occurrence of members thinner then the user defined MINDIM value in the optimization result. It would be of interest to see if OptiStruct is able to report how many members slightly smaller than MINDIM that remains. This information could then be used to consider the weight increase caused when these members are made thicker in the end of the development process. Otherwise the member sizes in each design have to be scanned to detect and count critical members. However, the best solution would be to develop an additional member size control which does not allow members to be smaller than the specified value. The member size control MINDIM is today considered as a manufacturing constraint. But, in my opinion I do not think it should be considered as a manufacturing constraint, since it in the same time permit members thinner than the prescribed minimum member size. Thus, it should rather be classified as an optimization control. Otherwise, I think the MINDIM should increase the thicknesses of these members, to fulfill manufacturing requirements.

It was unexpected to find the topology optimization result, with MINDIM 5 mm, lighter than the unconstrained topology optimization. This could either be due to the fact that TOPDISC is activated in the MINDIM 5 mm optimization and deactivated in the unconstrained optimization. Else, it could be related to differences of the violation grade between these two results i.e. how close the structural performance are to the structural constraints in the optimization. On the other hand, it could be seen in the output file (.out) that the unconstrained optimization had smaller margins to the structural constraints. Thus, the violation grade is not an explanation to why MINDIM 5 mm becomes lighter than the unconstrained optimization. Nevertheless, this result shows that the unconstrained topology optimization does not find the global optimum.

8.2 Topology result into C2C

One disadvantage, regarding the method of getting optimization result into casting simulation (Chapter 5), is the large volume increase which may be a source for inaccuracy in the results. The process is also done manually which is rather time consuming and should preferably be automated.

8.3 Methods to evaluate castability

The Niyama plots (Figure 6.2) was slightly hard to interpret. The Niyama results were the only results considering shrinkage defects and also the only castability criteria with a general threshold value.

This project showed that the solidification simulation results can be misleading if the liquid fraction is not taken into account. Hence, the liquid fraction turned out to be the solidification result with most potential to evaluate castability, but is disadvantaged by the fact that it is represented by an animation. Therefore, one of the most interesting findings in this thesis was that the temperature gradients can be used as a numerical substitute to the liquid fraction, since the liquid fraction is based on the temperature gradients. Hot spots can be detected by using the HotSpots tool on the temperature gradients (Subsection 6.1.4). Moreover, the HotSpots tool also has great potential to count the number of hot spots, but has to be further investigated to be used in a suitable manner.

Another important finding was that the casting results can be mapped to stresses. This is a highly relevant approach and is already used today, but not until in the end of the development process. This can now be done by the design engineers they self and also in a "numerical way". However, the mesh conversion, which was required in order to perform the stress-mapping, should be automated. Furthermore, the ordinary strength analysis should not be replaced by the stress-mapping analysis.

The choice of how to derive the rating value, which are based on the weighted values, must be handled with caution. The rating value is strongly dependent on which method that are used. Further investigations should be performed to find the most suitable weighting method in order to get as accurate rating value as possible. This could maybe be done by applying this method to even more already existing components and design in order to verify and improve the method. As well as, the method probably can be improved by choosing more established and realistic castability threshold values, which also has to be further studied. E.g. the impact of setting the criterion value $K16$ to either 1 or 0 could be an source of inaccuracy.

Since the total amount of nodes for the models differed, the fraction of the number-of-node-results and the total number of nodes was used for comparison. Though, this should not be considered as a fully accurate approach.

The disadvantage with the method presented in this thesis (Chapter 6) is though that the evaluation method does not bring out any general castability score. One single design concept can therefore not be graded separately. Yet, there are no response values with respect to castability that can connected to constraints and directly used in the topology optimization. If there were, it would be rather time consuming to integrate casting simulations in between each iteration of the structural optimization. Still, it would be very interesting to develop new casting manufacturing constraints. One suggestion is to integrate the casting design rules (Figure 2.3) into the topology optimization. This would not require any casting simulations in between the optimization iterations. Furthermore, the position of the feeders should preferably be chosen already in the early phase of the development process, in order to take these into account when designing against a directional solidification.

As described in Section 2.2 a large local solidification rate i.e. a fast solidification improves the mechanical properties. Thus, the solidification rate should be possible to use as an additional criterion. Since the starting temperature is the same for all nodes in the solidification simulation, the solidification rate can simply be derived from the end temperature in each node divided by the solidification time in each node.

9| Conclusions

The purpose of this master thesis was to find a development process for topology optimized casted components, where casting simulations and manufacturing constraints could be integrated in the early phase of the ordinary optimization process. It was of interest to find a way to sort among a large variety of different design concepts by evaluating castability numerically. Moreover, the aim was to find a way to get the topology optimization result into the casting simulation without realizing the geometry manually by using CAD.

In the beginning of this project it was discovered that the numerical results presented in C2C indicated that the Optimized Design was better than the Current RLCA from a casting point of view. This was rather surprising since it was already known that the Optimized Design was not feasible to cast. The only way to identify this fact was thus to look at the liquid fraction animations. But with the new methods, presented in Chapter 6, castability could be evaluated numerically which further determined the Current RLCA as the most beneficial from a casting point of view.

This project has shown that topology optimization result can be casting simulated without first being manually realized using CAD. Nevertheless, the final design still has to be realized in the end of the development process. However, it only has to be done once instead of for every single design concept. Furthermore, this thesis has also shown that casting properties can be evaluated numerically and that optimization results can be eliminated based on castability, already in the early phase of the development process.

9.1 Recommendations and Further Work

It is recommended that further research be undertaken in the following areas:

- Investigate in the possibility of integrating casting design rules as constraints in the topology optimization.
- Re-optimization: Investigate how modifications should be performed to still maintain an optimal design from both a strength and a castability point of view in a situation where the most optimal design concept has been found but still has to be slightly modified.
- Investigate why the topology optimization results sometimes contains loose hanging parts in the structure. Study if it might be related to the *no holes* option.
- Investigate in the possibility of capturing hot spots by tracking the directional change of the temperature gradient. E.g. by calculating the gradient of each (x, y, z) component of the temperature gradient.
- Find a method to count the number of features (ribs, members, holes etc.) of a design.
- Develop an optimization constraint, similar to the member size control MINDIM but with the only difference that it does not allow smaller members then the specified value.
- Perform further studies in order to solve the problem regarding the ribs that do not cohere properly when two design spaces are used. Investigate in why the structure always tend to turn 90 degrees to a free surface.
- The following processes are suggested to become automated:
  - method of getting the topology optimization result into casting simulation
  - mesh conversion

  - divide one design space into two design spaces and also implement a routine where the parting line between there two design spaces become optimized.
- Make further investigations regarding the searching distance dependence of the HotSpots tool. Find an accurate and consistent approach of counting the number of hot spots.

Bibliography

[1] ASM International. (2009, Nov.). *Casting Design and Performance.* [pdf]. Available: http://allaboutmetallurgy.com/wp/wp-content/uploads/2017/04/Designing-Castings-for-Performance.pdf [Jan. 23, 2018].

[2] R. Larsson. Master's Thesis. *Methodology for Topology and Shape Optimization: Application to a Rear Lower Control Arm.* Gothenburg, 2016.

[3] Kuang-O (Oscar) Yu. *Modeling for casting and solidification processing.* USA: Dekker, 2002.

[4] Steel Founders' Society of America. Steel Casting Handbook 2017.

[5] M. Di Sabatino and L. Arnberg. (2009, Oct). *Castability of aluminium alloys.* [pdf]. Vol. 62, Issues 4-5, page 321-325. Available: https://link.springer.com/article/10.1007/s12666-009-0049-2 [Jan. 23, 2018]

[6] E. Erlandsson, H. Johansson, N. Kåmark, P. Lundgren, M. Ögårg. (2015, June). Thesis report. *Topologi och formoptimerad lättviktsram till en quadcopter.* [pdf]. Available: http://publications.lib.chalmers.se/records/fulltext/218356/218356.pdf [Jan. 23, 2018]

[7] B.V Olho, Bendsoe, Rasmussen. On CAD-integrated structural topology and design optimization Computer Methods in Applied Mechanics and Engineering, (1991).

[8] M. Cenanovic. (2017). PhD Thesis. *Finite element methods for surface problems.* [pdf]. Available: http://hj.diva-portal.org/smash/get/diva2:1088644/FULLTEXT01.pdf [Jan. 23, 2018]

[9] P. Torne. (2016, May). *Casting Technologies.* [pdf]. Available: http://boeke-ie.de/wp-content/uploads/2016/07/Casting_Technologies_052616.pdf [Jan. 23, 2018].

[10] P. W. Christensen et al. *An introduction to structural optimization.* Linköping: Springer, 2009.

[11] M.P.Bendsøe O.Sigmund. *Topology Optimization Theory, Methods and Applications.* Berlin: Springer-Verlag, 2003.

[12] D. M. Stefanescu. *Science and Engineering of Casting Solidification - 3rd edition.* Swithzerland: Springer, 2015.

[13] D. M. Stefanescu. *Science and Engineering of Casting Solidification.* Switzerland: Springer, 2008.

[14] U. Kirsch. *Structural Optimization Fundamentals and Applications.* Berlin: Springer, 1993.

[15] Practical Aspects of Structural Optimization - A study guide. 2nd Edition. Altair University, 2015.

[16] Altair Connect, Internet: https://connect.altair.com/ [Jan. 23, 2018].

[17] G. Wei and Z. Miao-yong. *Characteristic Parameters for Dendritic Microstructure of Solidification During Slab Continuous Casting*, 2009. 17-21.

[18] I. Svensson and I. Svensson. *Gjuteriteknisk handbok.* Kalmar: Lenanders Grafiska AB. Swedish.

[19] B. Bourdin. *Filters in topology optimization.* Denmark: John Wiley Sons, Ltd, 2001.

[20] "Directional solidification" Internet: https://web.archive.org/web/2006121 0224324/http://www.energymanagertraining.com/foundries/pdf/CDA7.pdf, April 21, 2017 [Jan. 23, 2018].

[21] Wikipedia. "Topology optimization" Internet: https://en.wikipedia.org/wiki/Topology_optimization, Jan. 6, 2018 [Jan. 23, 2018].

[22] Wikipedia. “Casting (metalworking)” Internet: https://en.wikipedia.org/wiki/Casting_(metalworking), Jan. 3, 2018 [Jan. 23, 2018].
[23] Wikipedia. “Directional solidification” Internet: https://en.wikipedia.org/wiki/Directional_solidification, April 21, 2017 [Jan. 23, 2018].
[24] Wikipedia. “Chvorinov’s rule” Internet: https://en.wikipedia.org/wiki/Chvorinov’s_rule, Jan. 22, 2018 [Jan. 23, 2018].
[25] Wikipedia. “STL (file format)” Internet: https://en.wikipedia.org/wiki/STL_(file_format), Jan. 5, 2018 [Jan. 23, 2018].

A| Detailed settings

A.1 Topology optimization parameters

Initial Material Fraction [0,1]	0.9000
Minimum Element Volume Fraction	1.0000E-02
Discreteness Parameter	1.0000
Topology Optimization Method	Density Method
Maximum Number of Iterations	100
Convergence Tolerance	5.0000E-03
Step Size (Topology)	0.5000
Checkerboard Control	On (1 - Global Averaging)

Table A.1: Topology optimization parameters.

A.2 Casting parameters

A.2.1 Optimized Design and Current Design

Casting Method	Gravity casting
Gravity direction	none
Element size [mm]	1
Part Material	Aluminium AlSi7Mg
Part Temperature [^{o}C]	700
Mold Material	Steel-H13
Mold Temperature [^{o}C]	150
Use coating	no
Filling time [s]	15

Table A.2: C2C settings of the Optimized Design and Current Design.

A.2.2 Design concept B and C

inlet ⊘ [mm]:	10
Gravity direction	none
Casting Method	Gravity casting
Element size [mm]	3
Part Material	Aluminium AlSi7Mg
Part Temperature [^{o}C]	700
Mold Material	Steel-H13
Mold Temperature [^{o}C]	150
Use coating	no
gravity casting	yes
Filling time [s]	15

Table A.3: C2C settings of Design concept B and C.

B| C2C results

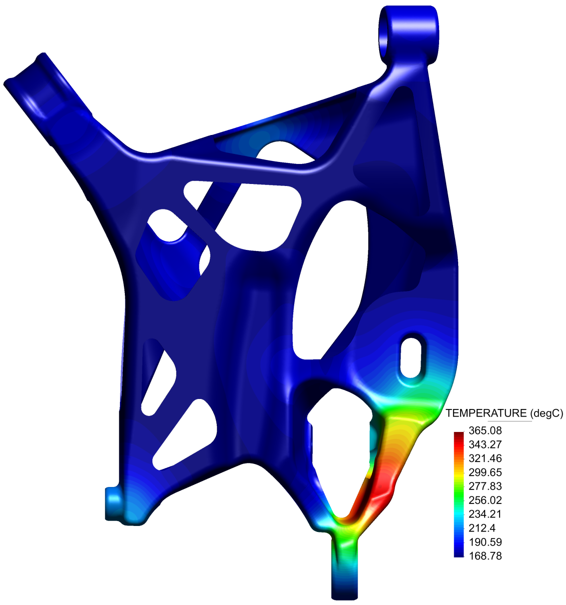

Figure B.1: Temperature results in C2C of the Optimized Design.

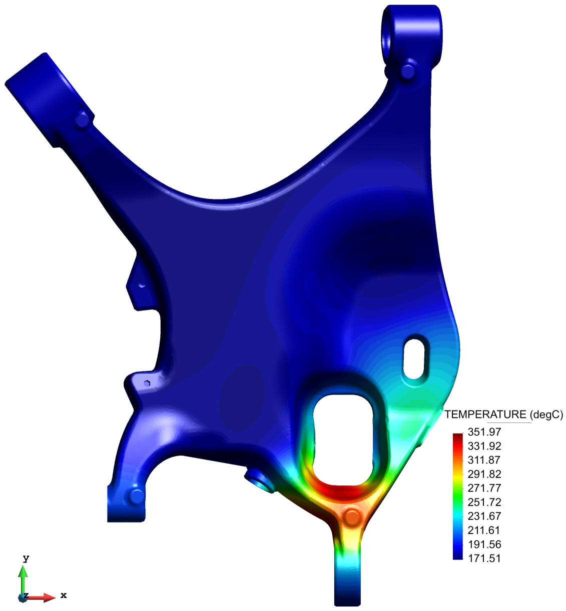

Figure B.2: Temperature results in C2C of the Current RLCA.

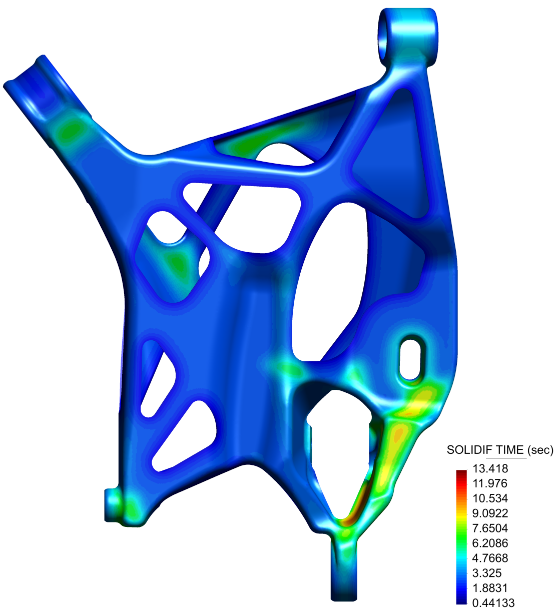

Figure B.3: Solidification results in C2C of the Optimized Design.

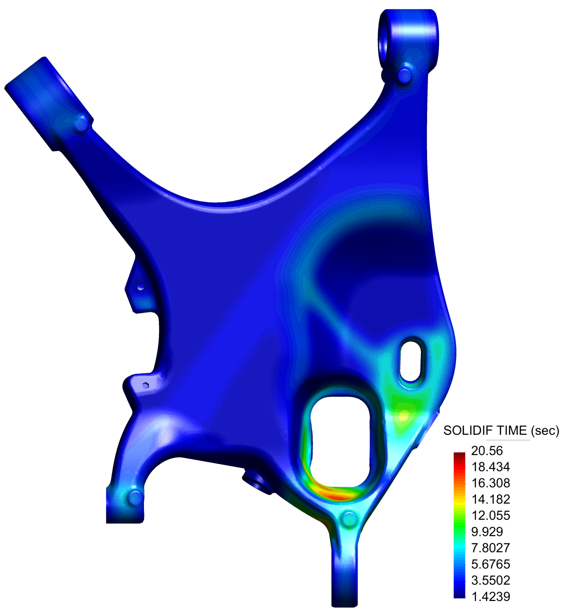

Figure B.4: Solidification results in C2C of the Current RLCA.

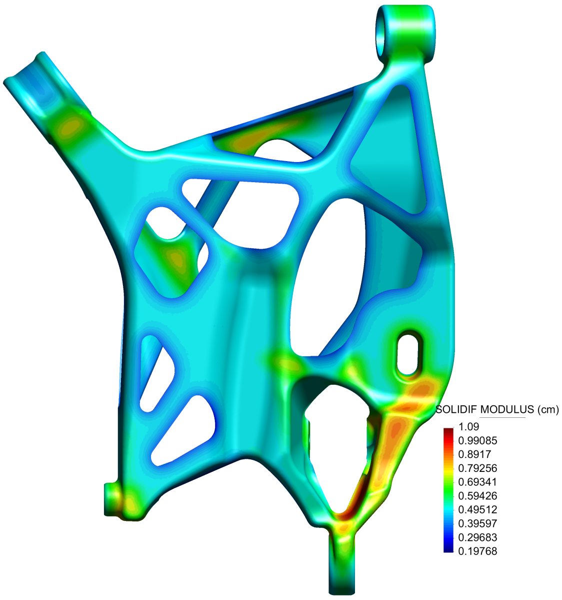

Figure B.5: Solidification Modulus results in C2C of the Optimized Design.

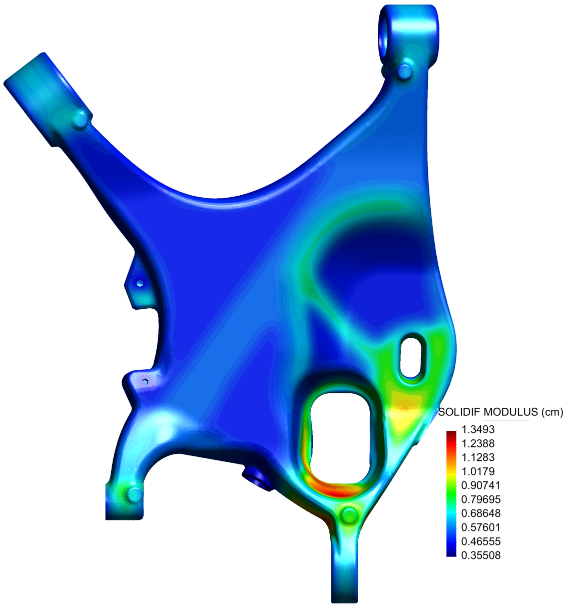

Figure B.6: Solidification Modulus results in C2C of the Current RLCA.

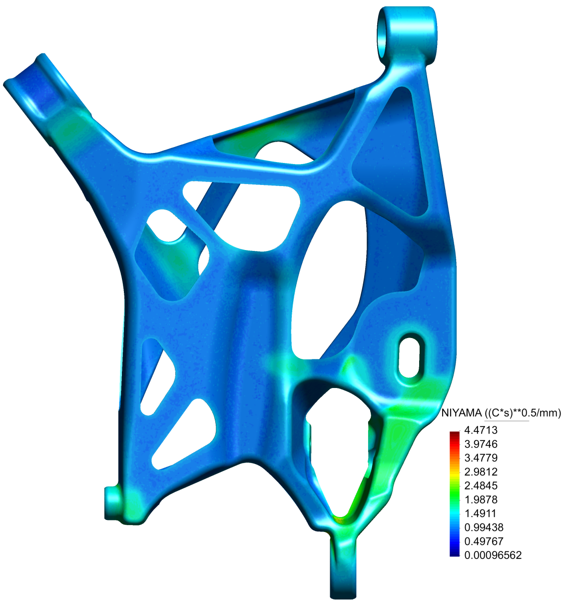

Figure B.7: Niyama results in C2C of the Optimized Design.

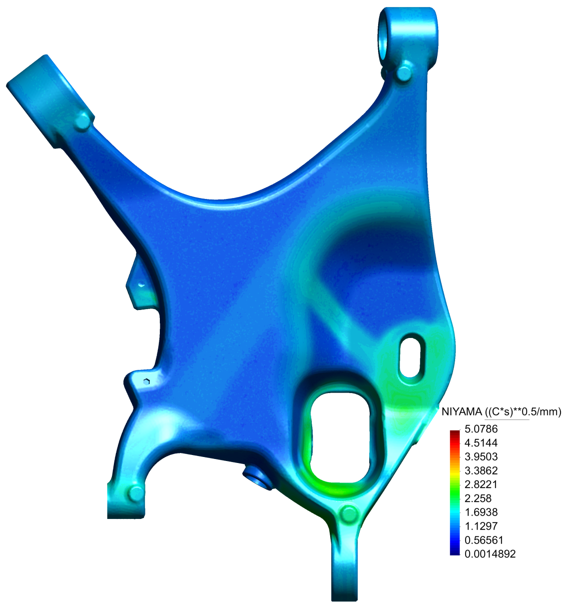

Figure B.8: Niyama results in C2C of the Current RLCA.

Figure B.9: Porosity 20% results in C2C of the Optimized Design.

Figure B.10: Porosity 20% results in C2C of the Current RLCA.

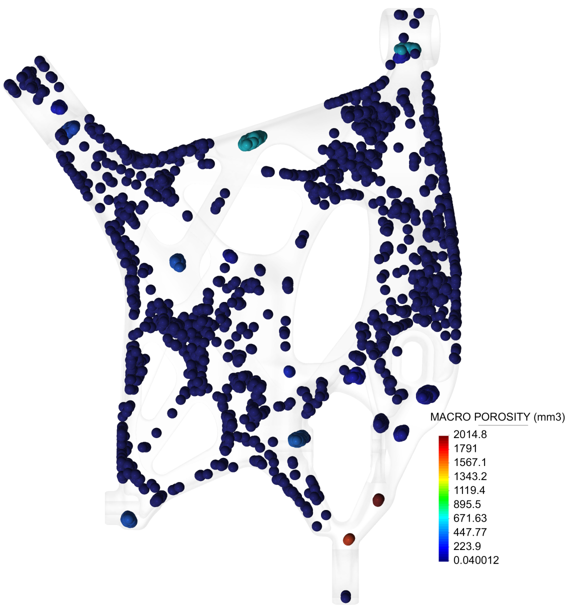

Figure B.11: Porosity results in C2C of the Optimized Design.

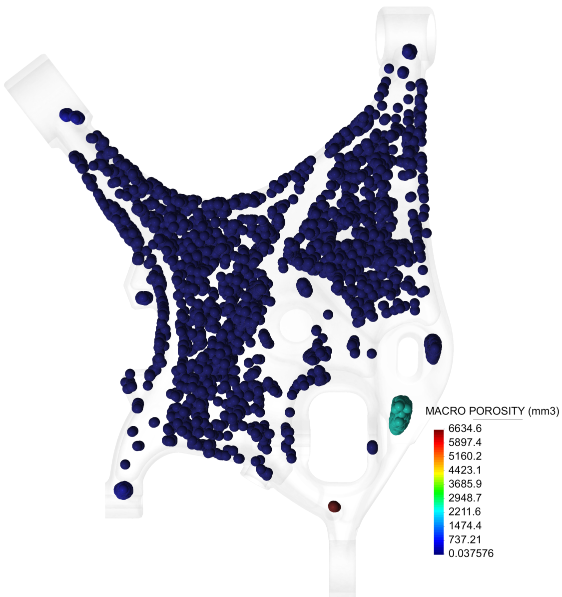

Figure B.12: Porosity results in C2C of the Current RLCA.